Journal Pre-proof

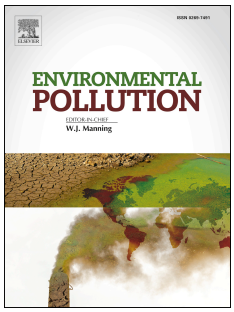

Significant decreases in the volatile organic compound concentrations, atmospheric oxidation capacity and photochemical reactivity during the National Day holiday over a suburban site in the North China Plain

Yuan Yang, Yonghong Wang, Dan Yao, Shuman Zhao, Shuanghong Yang, Dongsheng Ji, Jie Sun, Yinghong Wang, Zirui Liu, Bo Hu, Renjian Zhang, Yuesi Wang

PII: S0269-7491(19)37171-4

DOI: https://doi.org/10.1016/j.envpol.2020.114657

Reference: ENPO 114657

To appear in: *Environmental Pollution*

Received Date: 2 December 2019

Revised Date: 25 March 2020

Accepted Date: 22 April 2020

Please cite this article as: Yang, Y., Wang, Y., Yao, D., Zhao, S., Yang, S., Ji, D., Sun, J., Wang, Y., Liu, Z., Hu, B., Zhang, R., Wang, Y., Significant decreases in the volatile organic compound concentrations, atmospheric oxidation capacity and photochemical reactivity during the National Day holiday over a suburban site in the North China Plain, *Environmental Pollution* (2020), doi: https://doi.org/10.1016/j.envpol.2020.114657.

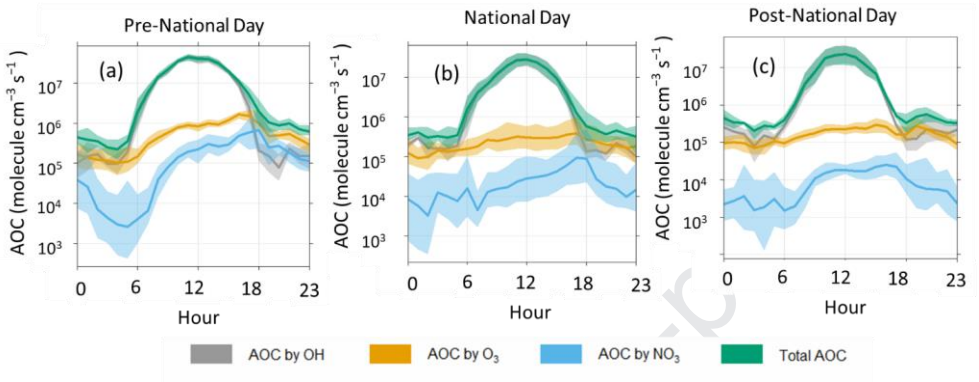

Significant Decreases in the Volatile Organic Compound Concentrations, Atmospheric Oxidation Capacity and Photochemical Reactivity during the National Day Holiday over a Suburban Site in the North China Plain

Yuan Yang[1,2], Yonghong Wang[3], Dan Yao[1,2,5], Shuman Zhao[1,2], Shuanghong Yang[1,4], Dongsheng Ji[1], Jie Sun[1], Yinghong Wang[1], Zirui Liu[1], Bo Hu[1], Renjian Zhang[1], Yuesi Wang[1,2,5*]

[1] Institute of Atmospheric Physics, Chinese Academy of Sciences, Beijing 100029, China

[2] University of the Chinese Academy of Sciences, Beijing 100049, China

[3] Institute for Atmospheric and Earth System Research / Physics, Faculty of Science, P.O.Box 64, 00014 University of Helsinki, Helsinki, Finland

[4] Department of Environmental Science and Engineering, Beijing University of Chemical Technology, Beijing 10029, China

[5] Center for Excellence in Regional Atmospheric Environment, Institute of Urban Environment, Chinese Academy of Sciences, Xiamen 361021, China

Submitted to: Environmental Pollution

Corresponding to: Yuesi Wang, wys@mail.iap.ac.cn;

Abstract

To what extent anthropogenic emissions could influence volatile organic compound (VOC) concentrations and related atmospheric reactivity is still poorly understood. China's 70th National Day holidays, during which anthropogenic emissions were significantly reduced to ensure good air quality on Anniversary Day, provides a unique opportunity to investigate these processes. Atmospheric oxidation capacity (AOC), OH reactivity, secondary transformation, O_3 formation and VOC-$PM_{2.5}$ sensitivity are evaluated based on parameterization methods and simultaneous measurements of VOCs, O_3, NO_x, CO, SO_2, $PM_{2.5}$, JO^1D, JNO_2, JNO_3 carried out at a suburban site between Beijing and Tianjin before, during, and after the National Day holiday 2019. During the National Day holidays, the AOC, OH reactivity, O_3 formation potential (OFP) and secondary organic aerosol formation potential (SOAP) were 1.6×10^7 molecules cm^{-3} s^{-1}, 41.8 s^{-1}, 299.2 μg cm^{-3} and 1471.8 μg cm^{-3}, respectively, which were 42%, 29%, 47% and 42% lower than pre-National Day values and -12%, 42%, 36% and 42% lower than post-National Day values, respectively. Reactions involving OH radicals dominated the AOC during the day, but OH radicals and O_3 reactions at night. Alkanes (the degree of unsaturation=0, (D, Equation 1)) accounted for the largest contributions to the total VOC concentration, oxygenated VOCs (OVOCs; D≤1) to OH reactivity and OFP, and aromatics (D=4) to the SOAP. O_3 production was identified as VOC-limited by VOC (ppbC)/NOx (ppbv) ratios during the sampling campaign, with greater VOC limitation during post- National Day and more-aged air masses during the National Day. The VOC-sensitivity coefficient (VOC-S) suggested that VOCs were more sensitive to $PM_{2.5}$ in low-pollution domains and during the National Day holiday. This study emphasizes the importance of not only the abundance, reactivity, and secondary transformation of VOCs but also the effects of VOCs on $PM_{2.5}$ for the development of effective control strategies to minimize O_3 and $PM_{2.5}$ pollution.

Key words: Atmospheric oxidation capacity; OH reactivity; Secondary transformation; VOC-sensitivity coefficient; National Day

1 Introduction

High concentrations of natural and anthropogenic O_3 and aerosol precursors influence radiative transfer, climate and urban air quality. (Bloss et al., 2005; Elshorbany et al., 2009; Wang

et al., 2019b; Wang et al., 2015b). Atmospheric oxidation capacity (AOC) controls the abundance of these precursors as well as the production rates of secondary pollutants (Elshorbany et al., 2009; Prinn, 2003). Hydroxyl radical (OH) activity accounts for the majority of AOC and initiates the oxidation of most precursors (Bloss et al., 2005; Levy, 1971). A quantitative measure of the oxidation capacity is derived from the rate of the total loss of all trace gases due to OH (Ehhalt et al., 2015), which is equivalent to the inverse of the OH lifetime and depends on the abundances and compositions of primary pollutants (Di Carlo et al., 2004; Ferracci et al., 2018). The necessity of quantifying AOC and OH reactivity has therefore become evident for understanding particle pollution and photochemical pollution.

The concentration of O_3, an important indicator and key measure of AOC (Cheng et al., 2008), shows increasing O_3 trends of 1-3 ppbv per year in megacity clusters in eastern China (Li et al., 2019b), reflecting an enhanced AOC during the recent summer season. O_3 is produced rapidly in polluted air by the reaction cycles involving VOCs and nitrogen oxides (NO_x= NO+NO_2) in the presence of solar radiation. Therefore, increasing/reducing emissions of key VOC species can reduce/increase the AOC of the troposphere. Different VOC species significantly differ in their potential to form O_3 (Carter, 2012). Technically, there are several parameterization approaches to estimate the chemical reactivity of ambient VOCs, including equivalent propene concentrations, OH loss frequency and maximum incremental reactivity (MIR). The O_3 formation potential (OFP), which is calculated based on MIR, is a direct method to assess the maximum contribution of VOC species to O_3 formation under optimum reaction conditions including high NOx concentration, high radiative flux and O_3 mainly derived from local production (Czader et al., 2008; Wu and Xie, 2017; Xue et al., 2017). Derived from emissions of speciated VOCs, the national OFP in China shows a persistent increasing trend with a growth factor of 2.6 during 1990–2017 (Li et al., 2019c) with maximum occurred in the North China Plain, Yangtze River Delta, and Pearl River Delta. Unsaturated compounds including m/p-xylene, ethylene, formaldehyde, toluene and propene were the species with the largest OFP contributions (Wu and Xie, 2017). Increasing OFP reflects, to some extent, increasingly severe O_3 pollution and enhanced AOC. In the context of reductions in critical pollutants such as NO_2, SO_2, CO and $PM_{2.5}$ (Sun et al., 2018; Zheng et al., 2018), identifying hotspots and major reactive VOC species is key to understanding the observed increasing O_3 trend and AOC.

Reportedly, increasing AOC can enhance SOA formation (Feng et al., 2019). Sensitivity studies show that the SOA decrease caused by reduced AOC is ubiquitous in the Beijing-Tianjin-Hebei (BTH) region and that their spatial relationship depends on the SOA precursor distribution (Feng et al., 2019). The propensity of different VOCs to form SOAs differs significantly and can be scaled to the SOA yield, fractional aerosol coefficient (FAC) and toluene-weighted mass contributions (Zhang et al., 2017). Derived from speciated VOCs, the BTH area and surroundings, the Yangtze River Delta, the Pearl River Delta, and the Sichuan-Chongqing District were found to have the highest SOA potential (SOAP), and toluene, n-dodecane, m/p-xylene, styrene, n-decane and n-undecane had the largest SOAP (Wu and Xie, 2018). Overall, identifying the major VOC contributors to SOA formation might provide useful insights for particulate pollution control.

National Day is one of the largest holidays in China, especially in 2019. The government held great ceremony in Beijing to celebrate the 70th anniversary of the People's Republic of China. To ensure good air quality during Anniversary Day on October 1, the local government enacted strict emission controls over the BTH area. The work focuses on the analysis of a comprehensive suite of data collected during an autumn field campaign carried out at a suburban site between Beijing and Tianjin. The temporal variations in VOC concentration, AOC, OH reactivity and secondary transformation of measured species were investigated. In addition, the temporal characteristics of O_3 formation and VOC-$PM_{2.5}$ sensitivity were determined. These results will help to understand the $PM_{2.5}$ pollution and O_3 pollution in suburban areas around the BTH area.

2 Methodology

2.1 Measurements

The sampling site is located at the Xianghe Atmospheric Observatory (39.798 °N, 116.958 °E; 15 m above sea level), a typical suburban site between Beijing and Tianjin, as depicted in Figure 1. The unique geographical location makes it an indispensable platform in Beijing air pollution warning system and plays an important strategic role in regional air pollution research (Sun et al., 2016b; Xin et al., 2015; Yang et al., 2019b). The sampling site is approximately 4 km west of the downtown center and is surrounded by residential areas and agricultural land. As observation platform, the station has carried on many science projects, such as MAX-DOAS SO_2 observations (Wang et al., 2014a), the "Strategic Priority Research Program" of the Chinese Academy of

Sciences including Category A and Category B (Xin et al., 2015). Samples were collected from September 20 to October 15, 2019. The VOCs instrument was placed in a room of a second-story building (10 m above the ground level) with an air conditioner. The measurement instrument of photolysis frequencies was installed in a room of a four-story building (15 m above the ground level). The measurement instruments of O_3, NOx, SO_2, CO and $PM_{2.5}$ were housed in a container about 50m south-west of the four-story building. Located between several megacities, the sampling sites experiences frequent pollution plumes and are subject to multiple source influences such as local emissions and regional transport from the urban areas (Sun et al., 2016b; Xin et al., 2015).

O_3, NOx, SO_2, and CO were measured using a UV photometric O_3 analyzer (model 49C/I, Thermo-Fisher Scientific, USA), chemiluminescence NOx analyzer (model 42C/I, Thermo-Fisher Scientific, USA), pulsed fluorescence SO_2 analyzer (model 43C/I, Thermo-Fisher Scientific, USA) and nondispersive infrared analyzer (model 48I, Thermo-Fisher Scientific, USA). The lowest detection limit, precision, zero drift, span drift and response time can be seen in (Tang et al., 2012; Wang et al., 2013; Wang et al., 2014b). $PM_{2.5}$ was measured by an RP1400a TEOM micro-oscillation balance ambient particulate monitor and detailed information can be seen in (Liu et al., 2015; Xin et al., 2012). The sampling methods and instrument protocols as well as quality assurance/quality control (QA/QC) procedures for air quality monitoring are described in detail in the Chinese National Environmental Protection Standard, Automated Methods for Ambient Air Quality Monitoring (HJ/T 193–2005; State Environmental Protection Administration of China, 2006). Ambient VOC samples were collected and analyzed continuously and automatically with a temporal resolution of 1 h using a custom-built gas chromatography-mass spectrometry/flame ionization detector (GC-MS/FID, Shimadzu, Japan). The measurement principle and quality assurance and control procedures were described in our previous study (Yang et al., 2019a). The photolysis frequencies, JO^1D, JNO_2 and JNO_3 in the atmosphere were measured by a PFS-100 photolysis spectrometer (Juguang Technology (Hangzhou) Co., Ltd., Hangzhou, China) (Wang et al., 2019a). Meteorological parameters were obtained from the National Meteorological Information Center (http://data.cma.cn/), including wind speed, wind direction, temperature and relative humidity with a temporal resolution of 2 minutes, which were averaged over 1-hour time intervals for the data evaluation.

2.2 Metrics and Parameterization methods

2.2.1 Degree of unsaturation

The degree of unsaturation (D), which is also known as "ring and double bond equivalent", can be calculated from the molecular formula as well as from any structural representation of a molecule corresponding to that molecular formula (Badertscher et al., 2001; Gilman et al., 2015; Murray et al., 2013) and is equal to

$$D = [2C + N - H + 2]/2 \quad (1)$$

where C, N, and H denote the number of carbons, nitrogen, and hydrogen atoms, respectively. The calculated D values of the measured VOC species are presented in Table S1 in the Supplementary material.

2.2.2 AOC

AOC is defined as the sum of oxidation rates of various primary pollutants (e.g., CO, CH_4, and VOCs) by various oxidants (e.g., OH, O_3 and NO_3 radicals) (Elshorbany et al., 2009; Geyer et al., 2001; Li et al., 2018; Xue et al., 2016). This study is limited to the oxidation of the measured CO and VOCs.

$$AOC = \sum_{i=1} k_{Y_i - X}[Y_i]\,[X] \quad (2)$$

Here, $[Y_i]$ and $[X]$ are mixing ratios of molecule Y_i and oxidant X, respectively. $k_{Y_i - X}$ is the rate constant of the oxidation of molecule Y_i with oxidant X. The higher the AOC, the higher the removal rate of most pollutants.

Simultaneous measurements of OH and NO_3 are not available in this study. OH radical concentration (in molecule cm^{-3}) can be estimated from the parameterization method suggested by (Ehhalt and Rohrer, 2000).

$$[OH] = a \times (J_{O^1D})^{\alpha} \times (J_{NO_2})^{\beta} \times \frac{b \times [NO_2] + 1}{c \times [NO_2]^2 + d \times [NO_2] + 1} \quad (3)$$

Here, J_{O^1D} and J_{NO_2} are the measured photolysis frequencies (s^{-1}) of O_3 and NO_2, respectively. The values of α=0.83, β=0.19, a=4.1×10^9, b=140, c=0.41 and d=1.7 were obtained from measurement data with NOx concentrations > 1 ppb during the POPCORN campaign at a rural site in Germany. $[NO_2]$ is measured NO_2 concentration (ppb). The method used here to estimated OH concentration has been used in other places of China (Lu et al., 2013; Yuan et al., 2013; Zheng

et al., 2011), and the uncertainty was within 50% according to the study by (Zheng et al., 2011) in North China Plain. Therefore, we think the method used to estimated OH concentration here is reasonable.

NO_3 concentration could be determined from steady-state assumption proposed by (Liebmann et al., 2018).

$$[NO_3] = \frac{k_{NO_2+O_3} \times [NO_2] \times [O_3]}{J_{NO_3} + k_{NO+NO_3} \times [NO] + L_{NO_3} + K_{ec} \times f_{ht} \times [NO_2]} \quad (4)$$

$$f_{ht} = \frac{\gamma \bar{c} A}{4} \quad (5)$$

Here, J_{NO_3} is the measured photolysis frequency (s^{-1}) of NO_3. L_{NO_3} (s^{-1}) is the VOC reactivity with NO_3. The rate coefficients for NO_2-O_3 ($k_{NO_2+O_3}$) and NO-NO_3 (k_{NO+NO_3}) were taken from the JPL-NASA Evaluation of Chemical Kinetics and Photochemical Data for Use in Atmospheric Studies (Atkinson et al., 2004) and are 3.5×10^{-17} and 2.6×10^{-11} cm^3 $molecule^{-1}$ s^{-1}, respectively. f_{ht} is the loss frequency due to the heterogeneous uptake of N_2O_5 to particles, which is approximately valid if the particles are less than ≈ 1μm in diameter. K_{ec} (=1.9×10^{-12} cm^3 $molecule^{-1}$ s^{-1}) is the equilibrium constant for NO_3 +NO_2 +M⇆N_2O_5 +M. γ (=0.022) is the dimensionless uptake coefficient taken from (Tham et al., 2018). $\bar{c}$ is the mean molecular velocity of N_2O_5 (26233 cm s^{-1} at 298 K). A is the aerosol surface area density (cm^2 cm^{-3}). detailed information can be seen in text S1 and Figures S1 and S2 in the Supplementary material.

2.2.3 Implications for atmospheric reactivity

The estimation of the impact on atmospheric chemistry of measured species is based on the three metrics including hydroxyl radical (OH) reactivity, O_3 formation potential (OFP) and secondary organic aerosol (SOA) formation potential, as shown in equations (6)-(8).

$$OH\ reactivity = \sum K_{OH+VOC_i}[VOC_i] + K_{OH+CO}[CO] + K_{OH+NO}[NO] + K_{OH+NO_2}[NO_2] + K_{OH+SO_2}[SO_2] + K_{OH+O_3}[O_3] + K_{OH+other}[other] \quad (6)$$

$$OFP_i = [VOC]_i \times MIR_i \quad (7)$$

$$SOAP = [VOC]_i \times SOAP_i \quad (8)$$

In the above equations, the rate coefficients K_{OH} (in cm^3 $molecule^{-1}$ s^{-1}) were taken from (Atkinson and Arey, 2003; Atkinson et al., 2006; Atkinson et al., 1997). MIR_i is the MIR of the i^{th} VOC species, which were from the report entitled "Estimation of Ozone Reactivities for Volatile Organic Compound Speciation Profiles in the Speciate 4.2 Database". $SOAP_i$ is the

potential of each VOC to form an SOA on a mass basis relative to the SOA formation potential of toluene, and its values were taken from (Derwent et al., 2010). $[VOC_i]$, $[CO]$, $[NO]$, $[NO_2]$, $[SO_2]$ and $[O_3]$ denote concentrations (in molecules cm^{-3}). The rate coefficients K_{OH}, MIR and $SOAP_i$ values of the measured VOC species are presented in Table S1 in the Supplementary material.

3 Results and discussion

3.1 Observational overview

In order to quantify the temporal variations of the AOC, OH reactivity and secondary transformation of measured species, three episodes are separately defined in this study: "pre-National Day" (September 20 to 30, 2019), National Day (October 1 to October 7, 2019), and "post-National Day" (October 8 to 15, 2019).

The mean diurnal profiles of major pollutants, photolysis frequencies and meteorological parameters during the three episodes are depicted in Figures 2 and S3. (the time series are shown in Figure S4 in the Supplementary material). The ambient temperature gradually decreased during the sampling period, with diurnal maxima of 28, 23 and 17□ during the pre-National Day, National Day and post-National Day, respectively. The observed wind patterns during the field campaign showed a predominant contribution from the north-west sector, with higher wind speed during the National Day. The photolysis frequencies JO^1D, JNO_2 and JNO_3 displayed similar diurnal variations, with the peak values occurring at approximately 12:00. However, JO^1D, JNO_2 and JNO_3 were highest during pre-National Day and comparable during the National Day and post-National Day episodes. The diurnal maximum O_3 concentration measured during the pre-National Day, National Day and post-National Day was 90 ppb, 55 ppb and 30 ppb, respectively. The diurnal cycle for the O_3 and $PM_{2.5}$ precursors CO, NO_x, and VOCs was opposite that of O_3, with mixing ratios varying by a factor of ~2 according to the time of day, but similar to that of $PM_{2.5}$. The diurnal patterns of the O_3 and $PM_{2.5}$ precursors were generally similar for the three episodes, with two obvious peaks during the morning and evening rush hour, which may result from elevated traffic emissions and lower consumption. In contrast, as depicted in Figure S3, the oxygenated VOC (OVOC; D=2) concentrations increased from a minimum near sunrise to a maximum in the late afternoon, reflecting the accumulation of OVOCs during the photochemically active period of the day.

The fractional composition and total concentration of measured VOCs are shown in Figure 3(a)-(c). The concentration of total VOCs (TVOCs) averaged 68.7 ppb during pre-National Day, was reduced to 43.5 ppb during the National Day episode, and increased to an average of 54.8 ppb during post-National Day. Thus, the concentration of TVOCs during the National Day was reduced by 37% compared with that pre-National Day and by 21% compared with that post-National Day. In the case of a diel cycle, alkanes (D=0) were the most abundant VOC group in all three periods, composing 33%, 35% and 33%, respectively, of the total, followed by OVOCs (D≤1) (27%, 24% and 24%) and halocarbons (D≤1) (17%, 18% and 18%). Although lower than that of alkanes, the contribution of alkenes (D= 1) increased over time, with this group composing 3%, 4% and 5% of the TVOCs during the pre-National Day, National Day and post-National Day, respectively. Compared with the pre-National Day values, the National Day levels of alkanes (D=0), alkanes (D=1), alkenes (D=1), alkenes (D=2), aromatics (D=4), aromatics (D=5), OVOCs (D≤1), OVOCs (D=2), halocarbons (D≤1), halocarbons (D=4) and acetylene (D=2) were decreased by approximately 34%, 34%, 19%, 33%, 41%, 39%, 44%, 38%, 32%, 28% and 34%, respectively, but that of acetonitrile (D=2) was increased by approximately 1%. Post-National Day, aromatics (D=5), aromatics (D=4) and alkenes (D=1) increased to the greatest extent, with enhancement factors of 1.5, 1.6 and 2.7, respectively, but alkenes (D=2), OVOCs (D=2) and halocarbons (D=4) decreased by approximately 4%, 11% and 37%, respectively, compared with the pre-National Day levels. Of the top 10 species in each episode, 8 were the same, including hexanal (D=1), propane (D=0), acetone (D=1), methylene chloride (D=0), ethane (D=0), n-butane (D=0), 1,2-dichloroethane (D=0) and acetylene (D=2), differing only in terms of rank order, as shown in Figure S5(a)-(c). Most of these species have lower degrees of unsaturation (D=0), which are less likely to react with atmospheric oxidants (OH, O_3 and NO_3 radicals), facilitating their accumulation. These species are mainly from fuel combustion and vehicle exhaust (Liu et al., 2017; Song et al., 2018); hence from perspective of the current emission-based limits, we recommend that the priorities for the control of VOC sources include fuel combustion and vehicle exhaust.

3.2 AOC

The calculated maximum AOC for pre-National Day, National Day and post-National Day was 8.5×10^7 molecules cm^{-3} s^{-1}, 4.9×10^7 molecules cm^{-3} s^{-1} and 7.1×10^7 molecules cm^{-3} s^{-1}, with

campaign-averaged values of 1.6×10^{7} molecules cm^{-3} s^{-1}, 9.3×10^{6} molecules cm^{-3} s^{-1} and 8.2×10^{6} molecules cm^{-3} s^{-1}, respectively. Obviously, the AOC was largest during pre-National Day, with a decreasing trend from pre-National Day to post-National Day. As such, the total number of CO and VOC molecules depleted during the day were 1.4×10^{12}, 8.0×10^{11} and 7.1×10^{11}, respectively, per cm^{-3} of air. Such AOC levels were lower than those determined at the Tung Chung air quality monitoring station (maximum AOC was up to 2.04×10^{8} and 1.27×10^{8} molecules cm^{-3} s^{-1} on 25 and 31 August, respectively) (Xue et al., 2016), and in a polluted area in Santiago, Chile with a peak of 3.2×10^{8} molecules cm^{-3} s^{-1} (Elshorbany et al., 2009), but comparable to those determined at the Hong Kong Polytechnic University's air monitoring station at Hok Tsui with maximum AOC levels up to 1.4×10^{8}, 6.2×10^{7} and 4.1×10^{7} molecules cm^{-3} s^{-1} in the late summer, autumn and winter, respectively(Li et al., 2018) and at the Jiangwan campus of Fudan University in northeast Shanghai with a peak of 8.8×10^{7} molecules cm^{-3} s^{-1} (Zhu et al., 2020).

During the National Day episode, the average AOC for OH, O_3 and NO_3 radicals throughout the entire day were 8.8×10^{6}, 1.0×10^{5} and 3.7×10^{5} molecule cm^{-3} s^{-1}, representing 95%, 4% and 1% of the total AOC, respectively. These values were 41%, 50% and 65% lower than those pre-National Day. The AOC presented similar diurnal variation patterns during the three episodes, with the maximum intensity at approximately noon and lower levels at night (Figure 4); due to the dominant contribution of OH to AOC, these patterns closely tracked with the diurnal variations of the calculated OH concentration (figures not shown) and solar radiation (as indicative of the observed JNO_2), in accordance with previous studies at other urban locales (Li et al., 2018; Zhu et al., 2020). The daytime average AOC was 2.3×10^{7} molecules cm^{-3} s^{-1}, 1.4×10^{7} molecules cm^{-3} s^{-1} and 1.2×10^{7} molecules cm^{-3} s^{-1}, while the nighttime average AOC was 6.4×10^{5} molecules cm^{-3} s^{-1}, 4.4×10^{5} molecules cm^{-3} s^{-1} and 4.1×10^{5} molecules cm^{-3} s^{-1} for pre-National Day, National Day and post-National Day, respectively. OH was, as expected, the predominant oxidant, accounting for 94%, 96% and 98% of the daytime (06:00-18:00 LT) AOC. O_3 was the second most important oxidant, with contributions of 4%, 3% and 2% during the pre-National Day, National Day and post-National Day (Figure 5). In comparison, NO_3 made only a minor contribution (2%, 1% and <1%). At night, O_3 was the major oxidant, accounting for 49%, 45% and 38% of the AOC, followed by OH (28%, 44% and 59%) and NO_3 (23%, 11% and 3%) during the pre-National Day, National Day and post-National Day, respectively, although the calculated nighttime NO_3

concentration were much higher than OH concentration. Compared with OH and O_3, NO_3 made a lower contribution during the day and at night, which was mainly caused by the high NO concentrations (Liebmann et al., 2018). We have emphasized that reactive Cl produced from $ClNO_2$ photolysis may contribute to AOC (Bannan et al., 2015; Xue et al., 2016), but this contribution was not quantitatively characterized in the present study.

3.3 Implications for atmospheric reactivity

3.3.1 OH reactivity of measured species

The calculated OH reactivity was categorized into the values for NO_2, NO, CO, SO_2, O_3 and VOCs. The average values during the National Day episode were 41.8 s^{-1}, which was 29% and 42% lower than those pre-National Day (59.1 s^{-1}) and post-National Day (72.2 s^{-1}), respectively. In general, the OH reactivity assessed in this study was much higher than that determined in Beijing (16.4 s^{-1}/20±11 s^{-1}), Shanghai (13.5 s^{-1}), Chongqing (17.8 s^{-1}), Jinan (19.4±2.1 s^{-1}), Wangdu (10-20 s^{-1}), Houston (9-22 s^{-1}), London (18.1 s^{-1}), Nashville (11.3 ± 4.8 s^{-1}), Guangzhou (22.7 s^{-1}), Heshan (31±20 s^{-1}), Backgarden (mean maximum value of 50 s^{-1}) and New York (25 s^{-1}) (Dolgorouky et al., 2012; Fuchs et al., 2017; Kovacs et al., 2003; Lou et al., 2010; Lyu et al., 2019; Mao et al., 2010; Ren et al., 2006; Tan et al., 2019; Whalley et al., 2016; Yang et al., 2017; Zhu et al., 2020), showing that the abundance of pollutants in Xianghe was much higher than that in other metropolitan areas of the world. During pre-National Day, NO_2 made the largest contribution to total OH reactivity (46%), followed by VOCs (26%), NO (15%), CO (13%), SO_2 (<1%) and O_3 (<1%). During the National Day, NO_2 accounted for the majority of total OH reactivity (47%), followed by VOCs (19%), CO (18%), NO (16%), SO_2 (<1%) and O_3 (<1%). During post-National Day, NO_2 and NO dominated the total OH reactivity (37% and 36%, respectively), followed by VOCs (17%), CO (10%), SO_2 (<1%) and O_3 (<1%).

The fractional composition and total OH reactivity of measured VOCs is shown in Figure 3(d)-(f). The total OH reactivity of the measured VOCs during the pre-National Day, National Day and post-National Day episodes were 15.2, 7.9 and 12.1 s^{-1}, respectively. In general, OVOCs (D≤1), OVOCs (D=2), alkenes (D=2), aromatics (D=4) and alkanes (D = 0) were major contributors to OH reactivity due to the relatively large concentration and rate coefficients for reaction with OH, accounting for ~90% of the total OH reactivity of measured VOCs in the three episodes, illustrating the importance of these groups in atmospheric photochemistry and O_3

generation. Of the top 10 species in each episode, 5 were the same, as shown in Figure S5 (d)-(f): hexanal (D=1), isoprene (D=2), m/p-xylene (D=4), acrolein (D=2), n-butanal (D=1), ethylene (D=1) and 1,3-butadiene (D=2). Most of these species are highly reactive with a variety of oxidants, and many of their oxidation products are photochemically active (Gilman et al., 2015). These species are mainly from traffic-related emissions, industry and solvent usage (Chen et al., 2014; Liu et al., 2017; Song et al., 2018). Therefore, in terms of OH reactivity-based limits, we recommend that the priorities for the control of VOC sources include traffic-related emissions, industry and solvent usage.

In general, the OH reactivity was lowest in the afternoon and highest during the morning and evening rush hour, as shown in Figure S6. Most campaigns have also reported slightly higher OH reactivity during morning rush hour, which can be explained by higher levels of reactive gases such as NO and VOCs due to heavy traffic (Dolgorouky et al., 2012; Fuchs et al., 2017; Mao et al., 2010; Ren, 2003; Ren et al., 2006; Williams et al., 2016; Yang et al., 2016). From a practical perspective, as depicted in Figure S6, NO_2, NO, CO, alkanes (D=0), alkanes (D=1), alkenes (D=1), alkenes (D=2), aromatics (D =4), aromatics (D=5), OVOCs (D≤1), acetonitrile (D=2) and acetylene (D=2) showed similar diurnal cycles, with minimum levels occurring at approximately 15:00 and peak values during morning and evening rush hour, which are typically connected to emissions from anthropogenic activities. The peak values of OH reactivity in the morning are mainly due to the increased NOx from rush hour traffic (Sheehy et al., 2010). The peak values during the night could be due to enhanced emissions that are released into the shallow nocturnal boundary layer (Fuchs et al., 2017). By contrast, the diurnal variations in O_3 and OVOCs (D=2) were inversely related to those of the above groups. The O_3 and OVOC (D=2) concentrations scaled with the photochemical parameters; hence, maximum mixing ratios were reached in the afternoon. The diurnal profiles of O_3 and OVOCs partly counteracted the decrease in OH reactivity in the afternoon due to the decreases in NO_x, CO, alkanes, alkenes, aromatics, acetonitrile and acetylene.

3.3.2 OFP of measured species

The fractional composition and total OFP of the measured VOCs are shown in Figure 3(g)-(i). Clearly, the OFP of TVOCs was much lower (299.2 μg cm^{-3}) during the National Day than during the pre-National Day (567.2 μg cm^{-3}) and post-National Day (466.4 μg cm^{-3}). Thus, the OFP of

TVOCs was 47% and 36% lower during the National Day than during the pre-National Day and post-National Day. Overall, the OFP was dominated by OVOCs (D≤1) and aromatics (D=4), together constituting 56% to 67%, during the three episodes, followed by OVOCs (D=2) (8%-15%) and alkanes (D=0) (10%-12%). Unsaturated OVOCs and saturated aromatics composed the dominant fraction during the three episodes due to their relatively large concentration and/or high MIR values in the atmosphere (Atkinson and Arey, 2003; Sommariva et al., 2011). The top 10 VOCs contributing to the OFP during the three episodes are shown in Figure S5 (g)-(i). These 10 species contributed approximately 72%, 67%, and 73% to the total OFP in the three cases, respectively. The top 10 VOCs were unsaturated compounds (D≥1), which are more likely to react with atmospheric oxidants, making unsaturated species potentially important O_3 precursors (Gilman et al., 2015). The top 10 VOCs are mainly from traffic-related emissions and solvent usage (Chen et al., 2014; Liu et al., 2017; Song et al., 2018). Therefore, in terms of OFP-based limits, we recommend that the priorities for the control of VOC sources include traffic-related emissions and solvent usage.

3.3.3 SOA formation potential of measured species

According to our estimates, the National Day episode had the lowest SOA potential (1471.8 μg cm^{-3}) compared to that during the pre-National Day and post-National Day, which had 1.7 and 1.7 times greater estimated SOAP values, respectively, as shown in Figure 3(j)-(l). Overall, aromatics (D=4), such as m/p-xylene, toluene, benzene, o-xylene, ethylbenzene, m-ethyltoluene, o-ethyltoluene, p-ethyltoluene and n-propylbenzene, and aromatics (D=5) accounted for the largest contributions to the SOAP, which is consistent with previous studies (Dominutti et al., 2019; Song et al., 2018; Wu and Xie, 2018). Generally, the tendency for aerosol formation increased as the size and polarity of VOCs increased because the size and polarity of VOCs has fundamental effects on the vapor pressure of molecules (Han et al., 2018; Kroll and Seinfeld, 2008). The initiation mechanism dominates the oxidation of aromatics, so the predominant products contain two polar functional groups (Jang et al., 2006; Lambe et al., 2012). Conversely, SOA formation from alkanes involves functionalization and fragmentation (Lambe et al., 2012), although alkanes accounted for the largest contributions to the TVOC concentration. The top 10 species constituted 97%, 97% and 98% of the total OFP during the pre-National Day, National Day and post-National Day, respectively, as shown in Figure S5 (j)-(l). Traditionally, these species

are thought to have the largest propensity to form SOAs, although the levels of predicted SOAs are typically much lower than those observed in ambient air (de Gouw et al., 2005; Volkamer et al., 2006). It is known that these species can be emitted from vehicular exhaust or associated with the solvent emissions of paints, inks, sealant, varnish and thinner for architecture and decoration (Ait-Helal et al., 2014; Liu et al., 2017; Liu et al., 2008; Wang et al., 2015a; Yang et al., 2019a). Therefore, in terms of SOA-based limits, we recommend that the priorities for the control of VOC sources include vehicular exhaust and solvent usage.

3.4 Photochemical age and O_3

[OH]×Δt named OH exposure (Jimenez et al., 2009), the product of OH radical concentration [OH] and reaction time Δt for the VOCs in the atmosphere between emission source and receptor, is derived from the photochemical age (Yuan et al., 2012). The photochemical age is usually calculated with two different methods: first, by employing the ratio of two compounds of same origin with different rate coefficients towards OH, e.g., propene and ethene, n-butane and propane, iso-butane and propane, benzene and toluene, m/p-xylenes and benzene, ethylbenzene and m/p-xylenes, benzene and 1,2,4-trimethylbenzene (Borbon et al., 2013; Chen et al., 2016; de Gouw et al., 2017; de Gouw et al., 2005; Ensberg et al., 2014; Hayes et al., 2013; Jimenez et al., 2009; Laurila and Hakola, 1996; Nelson and Quigley, 1983; Parrish et al., 1998; Roberts et al., 1984; Sun et al., 2016a; Warneke et al., 2007; Yuan et al., 2012), and second, by defining the photochemical age as $\log_{10}(NO_x/NO_y)$ (Hayes et al., 2013; Kleinman et al., 2008). Despite some limitations and substantial uncertainties (McKeen et al., 1996; Parrish et al., 2007), those ratios not merely yield useful measures of photochemical processing in the troposphere, but provide useful test of the treatment of mixing and chemical processing in chemical transport models (Parrish et al., 2007). In this study, the aromatic isomers m/p-Xylenes and ethylbenzene are the two VOCs used here in the calculation of the photochemical age (Guo et al., 2007; So and Wang, 2004; Zhang et al., 2008). It is based on three facts established by (Nelson and Quigley, 1983): 1) these compounds occur in significant concentrations and constant relative proportion in the major anthropogenic sources of hydrocarbons, 2) the compounds disappear from the atmosphere at markedly different rates by photochemical reaction and 3) various sources of these two species tend to have a similar ratio of about 3.6.

$$[OH] \times \Delta t = \frac{1}{\left(k_{m/p-xylenes} - k_{ethylbenzene}\right)} \times \left[\ln \frac{[m/p-xylenes]}{[ethylbenzene]}\Big|_{t=0} - \ln \frac{[m/p-xylenes]}{[ethylbenzene]}\Big|_{t}\right] \quad (9)$$

where the parameters $k_{m/p-xylenes}$ and $k_{ethylbenzene}$ are rate constants of m/p-xylene and ethylbenzene, respectively. $\frac{[m/p-xylenes]}{[ethylbenzene]}\Big|_{t}$ is the measured ratio of m/p-xylenes/ethylbenzene. $\frac{[m/p-xylenes]}{[ethylbenzene]}\Big|_{t=0}$ is the initial ratio of m/p-xylenes to ethylbenzene. As presented in Figure S7, we chose 3.54, 3.48 and 3.95 ppb ppb^{-1} as initial emission ratios of ethylbenzene to m/p-xylene for the pre-National Day, National Day, and post-National Day, respectively, as they were the largest ratios for the diurnal variations during the three episodes. The diurnal maximum OH exposure was calculated as 3.7×10^{10} molecules s cm^{-3}, 2.8×10^{10} molecules s cm^{-3} and 1.5×10^{10} molecules s cm^{-3} during the National Day, pre- and post-National Day, respectively, as shown in Figure 6a, indicating a more-aged atmospheric environment during the National Day holiday.

Generally, higher O_3 concentrations are indicative of greater photochemical age. Figure 6b shows the relationship between the OH exposure and O_3 concentration. During the three episodes, higher O_3 mixing ratios coincided with greater OH exposure, although O_3 seemed to be not highly correlated with photochemical age. The relatively poor correlation during the National Day (R^2= 0.35) and post-National Day (R^2=0.27) may indicate that the entrainment of air from the O_3-rich residual layer trapped aloft is important to the accumulation of surface O_3 during the two episodes (Xu et al., 2011).

3.5 VOC-NO_x-O_3 sensitivity

The VOC (ppbC)/NO_x (ppbv) ratio is often used to determine the O_3 formation sensitivity (Li et al., 2019a; Zou et al., 2015) based on experiential criteria in previous studies and the transition from VOC-limited to NO_x-limited conditions at a VOC (ppbC)/NO_x (ppbv) ratio of approximately 8:1 (Seinfeld, 1989). The daily mean value of the VOC (ppbC)/NO_x (ppbv) ratio was 8.4, 7.2 and 5.0 during the pre-National Day, National Day and post-National Day, respectively, indicating that the production of O_3 was more sensitive to VOCs during the post-National Day than during the National Day and pre-National Day due to the presence of strong NO_x emissions. Considering that the impact of VOCs on ozone formation was more closely related to the reactivity of individual VOC species than to the amount of total VOCs, defining O_3 production regimes in terms of the OH reactivities of VOCs and NOx is also a way of assessing the sensitivity of O_3 production to the

prevailing conditions. (Kirchner et al., 2001; Lyu et al., 2019; Pfannerstill et al., 2019; Sinha et al., 2012). The O_3 production regime plot, as illustrated in Figure S8, showed that the three episodes were characterized by strong VOC limitation. The higher the O_3 concentration is, the more obvious the VOC limitation. Overall, the results suggested that O_3 formation was more likely to be VOC-limited during the three episodes; hence reduction in VOC emission or increase in NOx emission can increase O_3 reduction.

From the daily variations in the VOC/NO_x ratio (Figure 7a), higher ratios were observed at night, exceeding 8:1, especially during the pre-National Day and National Day. These observations suggested more emission sources of VOCs at night, resulting in the O_3 formation system shifting to NOx-limited. O_3 formation depends not only on the abundance of precursors but also on the VOC/NO_x ratio (Li et al., 2019a). However, there were no discernible relationship (R^2<0.1) between O_3 and VOC/NOx occurred during the three episodes, as depicted in Figure 7b, possibly due to the counteraction of other uncertain factors. It should be noted the analysis is only approximate in terms of the assessment of VOC or NOx limitations for O_3 control because the VOC (ppbC)/NOx (ppbv) ratio indicator obtained from the numerical simulations of O_3 pollution in Los Angeles in the 1980s, which may be different from the air measured in Xianghe. Further investigation based on a photochemical model and more accurate measurements of VOCs and NOx is needed in the future to obtain more robust conclusions.

3.6 VOC–$PM_{2.5}$ sensitivity

In general, the relationship of VOC concentrations with the $PM_{2.5}$ concentration displayed similar trends, as shown in Figure S9. The above trends were useful indicators of qualitative relationships but cannot quantitatively reveal the pattern of variation. Rather than a simple concentration comparison, we used a gradient model (Equation 10), which used a $PM_{2.5}$-dependent function to incorporate data from pre-National day to post-National day, to investigate the relationship between VOC and $PM_{2.5}$ concentrations. The partitioning of atmospheric VOCs between gaseous and particulate phases is affected by particulate matter concentrations and other factors. Here, we propose a VOC-sensitivity coefficient (VOC-S) (Equation 10) to evaluate the degree to which VOC concentrations were influenced by the $PM_{2.5}$ concentration (Han et al., 2017; Han et al., 2018). Detailed descriptions of the gradient model and VOC-sensitivity coefficient can be seen in the text S2 in supporting Information.

$$\eta = \frac{\Delta_{VOCs}}{\Delta_{PM_{2.5}}} \quad (10)$$

$$\text{VOCs–S} = \frac{\eta_{\Delta}}{\eta_{B}} = \frac{\Delta_{VOCs}/B_{VOCs}}{\Delta_{PM_{2.5}}/B_{PM_{2.5}}} \quad (11)$$

where Δ_{VOCs}, $\Delta_{PM_{2.5}}$, B_{VOCs}, and $B_{PM_{2.5}}$ represent the concentrations of VOCs and $PM_{2.5}$ in specific $PM_{2.5}$ gradients and the background concentrations of VOCs and $PM_{2.5}$, respectively. In this study, the average $PM_{2.5}$ concentrations in the <5 μg m^{-3} domain were considered $B_{PM_{2.5}}$, and the corresponding mean VOC concentration was regarded as B_{VOCs}. The larger the VOCs–S value, the more sensitive the VOC concentrations were to $PM_{2.5}$, which means that VOC concentrations could exhibit major changes, while $PM_{2.5}$ concentrations only displayed minor variations.

To examine the variation in the level of sensitivity of VOCs to $PM_{2.5}$, VOCs and $PM_{2.5}$ were subdivided into 16, 14 and 12 groups on the basis of concentration in intervals of 5 μg m^{-3} $PM_{2.5}$ during the pre-National Day, National Day, and post-National Day, respectively. The mean VOC-S coefficient of VOCs in each group were plotted against R (the ratio of $\Delta_{PM_{2.5}}$ to $B_{PM_{2.5}}$) and were fitted with a typical power function:

$$y = a \times x^{b} \quad (12)$$

where x and y represent R and VOC-S, respectively, and a and b are regression parameters. As shown in Figure 8, a statistically significant relationship was found between VOC-S and R, with fitted r^2 values of 0.97 ($p < 0.001$), 0.92 ($p < 0.001$) and 0.72 ($p < 0.001$) during the pre-National Day, National Day, and post-National Day, respectively. Overall, the low VOC-S values in each episode remained almost constant, while the high VOC-S values displayed a steadily decreasing trend, suggesting that VOCs were more sensitive to $PM_{2.5}$ in low-pollution domains. The parameter m, which is the slope of the linear regression between ln (Δ_{VOCs}/B_{VOCs}) and ln ($\Delta_{PM_{2.5}}/B_{PM_{2.5}}$) and equal to "1+ b", revealed more information, such as differences among VOC species and temporal variations (Han et al., 2018), reducing the possible bias resulting from comparing only concentrations (Han et al., 2017). As depicted in Figure S10, TVOCs produced similar results, with m values of 0.34, 0.68 and 0.56 during the pre-National Day, National Day, and post-National Day, respectively, indicating that TVOCs were less sensitive to $PM_{2.5}$ during the pre-National Day than during the National Day and post-National Day.

The VOC-S values of alkanes (D=0), alkenes (D=1), alkenes (D=2), aromatics (D=4), aromatics (D=5), OVOCs (D≤1), and acetylene (D=2) were also investigated, and the results were

similar to the TVOC results, as shown in Figures S11-S17. Pre-National Day, alkenes (D=1) had stronger effects on $PM_{2.5}$, with an m value of 0.61, followed by aromatics (D=4), aromatics (D=5), alkanes (D=0), acetylene (D=2), OVOCs (D≤1) and alkenes (D=2), as shown in Figure S10. During the National Day, alkanes (D=0) and acetylene (D=2) had comparable effects on $PM_{2.5}$, as they did during post-National Day. Therefore, although aromatics (D=4) and aromatics (D=5) accounted for the largest contributions to the SOAP, both were less sensitive to $PM_{2.5}$, especially during the National Day and post-National Day. In contrast, alkanes (D=0) and acetylene (D=2) made smaller contributions to the SOAP, but both were more sensitive to $PM_{2.5}$. These results indicated that further study on SOA formation should take into account the properties of specific VOC.

4 Conclusions

In this study, we comprehensively analyzed the variations in AOC, OH reactivity, secondary transformation, O_3 formation and VOC-$PM_{2.5}$ sensitivity based on parameterization methods and simultaneous measurements of major pollutants, photolysis frequencies and meteorological parameters at a suburban site between Beijing and Tianjin before, during, and after National Day 2019. The diurnal cycle of CO, NO_x, and VOCs was opposite that of O_3, but similar to that of $PM_{2.5}$ during the three episodes. During the National Day holidays, the TVOC concentration, AOC, OH reactivity, OFP and SOAP were lower than pre-National Day and post-National Day values. Overall, the concentrations of alkanes (D=0) were higher than that of other groups, however, OVOC (D≤1) and aromatics (D=4) made larger contributions for OH reactivity, OFP and SOAP. OH radicals dominated the AOC during the day, but OH radicals and O_3 reactions at night. OH reactivity presented similar diurnal variation patterns during the three episodes with lowest in the afternoon and highest during the rush hour. The O_3 photochemical formation regime during the three episodes was identified as VOCs-limited by VOC (ppbC)/NO_x (ppbv) ratios, with greater VOC limitation during the post-National Day and more-aged atmospheric environment during the National Day holiday. VOC-S coefficient indicated VOCs were more sensitive to $PM_{2.5}$ in low-pollution domains and during the National Day holiday. Alkenes (D=1) and aromatics (D=4) were more sensitive to $PM_{2.5}$ pre-National Day, but alkanes (D=0) and acetylene (D=2) during the National Day and post-National Day.

Acknowledgment

This study was financially supported by the Ministry of Science and Technology of China [grant number 2017YFC0210000]; Beijing Major Science and Technology Project [grant number Z181100005418014]; and National Research Program for key issues in air pollution control [grant number DQGG0101]. All referenced supplemental figures and tables can be found in the supporting information. The authors are grateful to all staff and workers at the Xianghe Atmospheric Observatory for their support during the sampling campaign. We also acknowledge the National Meteorological Information Center for providing high-quality meteorological data.

References

Ait-Helal, W., Borbon, A., Sauvage, S., Gouw, J.A.d., Colomb, A., Gros, V., Freutel, F., Crippa, M., Afif, C., Baltensperger, U., Beekmann, M., Doussin, J.-F., Durand-Jolibois, R., Fronval, I., Grand, N., Leonardis, T., Lopez, M., Michoud, V., Miet, K., Perrier, S., Prévôt, A.S.H., Schneider, J., Siour, G., Zapf, P., Locoge, a.N., 2014. Volatile and intermediate volatility organic compounds in suburban Paris: variability, origin and importance for SOA formation. Atmospheric Chemistry and Physics 14, 10439-10464.

Atkinson, R., Arey, J., 2003. Atmospheric Degradation of Volatile Organic Compounds. Chemical Reviews 103, 4605-4638.

Atkinson, R., Baulch, D.L., Cox, R.A., Crowley, J.N., Hampson, R.F., Hynes, R.G., Jenkin, M.E., Rossi, M.J., Troe, J., 2004. Evaluated kinetic and photochemical data for atmospheric chemistry: Volume I - gas phase reactions of Ox, HOx, NOx and SOx species. Atmos. Chem. Phys. 4, 1461-1738.

Atkinson, R., Baulch, D.L., Cox, R.A., Crowley, J.N., Hampson, R.F., Hynes, R.G., Jenkin, M.E., Rossi, M.J., Troe, J., 2006. Evaluated kinetic and photochemical data for atmospheric chemistry: Volume II-gas phase reactions of organic species. Atmospheric Chemistry and Physics 6, 3625-4055.

Atkinson, R., Baulch, D.L., Cox, R.A., Hampson, R.F., Kerr, J.A., Rossi, M.J., Troe, J., 1997. Evaluated Kinetic and Photochemical Data for Atmospheric Chemistry: Supplement VI. IUPAC Subcommittee on Gas Kinetic Data Evaluation for Atmospheric Chemistry. Journal of Physical and Chemical Reference Data 26, 1329-1499.

Badertscher, M., Bischofberger, K., Munk, M.E., Pretsch, E., 2001. A novel formalism to

551 characterize the degree of unsaturation of organic molecules. J Chem Inf Comput Sci 41, 889-893.
552 Bannan, T.J., Booth, A.M., Bacak, A., Muller, J.B.A., Leather, K.E., Le Breton, M., Jones, B.,
553 Young, D., Coe, H., Allan, J., Visser, S., Slowik, J.G., Furger, M., Prevot, A.S.H., Lee, J.,
554 Dunmore, R.E., Hopkins, J.R., Hamilton, J.F., Lewis, A.C., Whalley, L.K., Sharp, T., Stone, D.,
555 Heard, D.E., Fleming, Z.L., Leigh, R., Shallcross, D.E., Percival, C.J., 2015. The first UK
556 measurements of nitryl chloride using a chemical ionization mass spectrometer in central London
557 in the summer of 2012, and an investigation of the role of Cl atom oxidation. Journal of
558 Geophysical Research-Atmospheres 120, 5638-5657.
559 Bloss, W.J., Evans, M.J., Lee, J.D., Sommariva, R., Heard, D.E., Pilling, M.J., 2005. The oxidative
560 capacity of the troposphere: Coupling of field measurements of OH and a global chemistry
561 transport model. Faraday Discussions 130, 425-436.
562 Borbon, A., Gilman, J.B., Kuster, W.C., Grand, N., Chevaillier, S., Colomb, A., Dolgorouky, C.,
563 Gros, V., Lopez, M., Sarda-Esteve, R., Holloway, J., Stutz, J., Petetin, H., McKeen, S., Beekmann,
564 M., Warneke, C., Parrish, D.D., de Gouw, J.A., 2013. Emission ratios of anthropogenic volatile
565 organic compounds in northern mid-latitude megacities: Observations versus emission inventories
566 in Los Angeles and Paris. Journal of Geophysical Research: Atmospheres 118, 2041-2057.
567 Carter, W.P.L., 2012. Development of Ozone Reactivity Scales for Volatile Organic Compounds.
568 Air & Waste 44, 881-899.
569 Chen, W., Shao, M., Wang, M., Lu, S., Liu, Y., Yuan, B., Yang, Y., Zeng, L., Chen, Z., Chang,
570 C.-C., Zhang, Q., Hu, M., 2016. Variation of ambient carbonyl levels in urban Beijing between
571 2005 and 2012. Atmospheric Environment 129, 105-113.
572 Chen, W.T., Shao, M., Lu, S.H., Wang, M., Zeng, L.M., Yuan, B., Liu, Y., 2014. Understanding
573 primary and secondary sources of ambient carbonyl compounds in Beijing using the PMF model.
574 Atmospheric Chemistry and Physics 14, 3047-3062.
575 Cheng, Y., Wang, X., Liu, Z., Bai, Y., Li, J., 2008. A new method for quantitatively characterizing
576 atmospheric oxidation capacity. Science in China Series B: Chemistry 51, 1102-1109.
577 Czader, B.H., Byun, D.W., Kim, S.T., Carter, W.P.L., 2008. A study of VOC reactivity in the
578 Houston-Galveston air mixture utilizing an extended version of SAPRC-99 chemical mechanism.
579 Atmospheric Environment 42, 5733-5742.
580 de Gouw, J.A., Gilman, J.B., Kim, S.W., Lerner, B.M., Isaacman-VanWertz, G., McDonald, B.C.,

581 Warneke, C., Kuster, W.C., Lefer, B.L., Griffith, S.M., Dusanter, S., Stevens, P.S., Stutz, J., 2017.
582 Chemistry of Volatile Organic Compounds in the Los Angeles Basin: Nighttime Removal of
583 Alkenes and Determination of Emission Ratios. Journal of Geophysical Research: Atmospheres
584 122, 11843-11861.
585 de Gouw, J.A., Middlebrook, A.M., Warneke, C., Goldan, P.D., Kuster, W.C., Roberts, J.M.,
586 Fehsenfeld, F.C., Worsnop, D.R., Canagaratna, M.R., Pszenny, A.A.P., Keene, W.C., Marchewka,
587 M., Bertman, S.B., Bates, T.S., 2005. Budget of organic carbon in a polluted atmosphere: Results
588 from the New England Air Quality Study in 2002. Journal of Geophysical Research 110, D16305.
589 Derwent, R.G., Jenkin, M.E., Utembe, S.R., Shallcross, D.E., Murrells, T.P., Passant, N.R., 2010.
590 Secondary organic aerosol formation from a large number of reactive man-made organic
591 compounds. Science of the Total Environment 408, 3374-3381.
592 Di Carlo, P., Brune, W.H., Martinez, M., Harder, H., Lesher, R., Ren, X., Thornberry, T., Carroll,
593 M.A., Young, V., Shepson, P.B., Riemer, D., Apel, E., Campbell, C., 2004. Missing OH reactivity
594 in a forest: evidence for unknown reactive biogenic VOCs. Science 304, 722-725.
595 Dolgorouky, C., Gros, V., Sarda-Esteve, R., Sinha, V., Williams, J., Marchand, N., Sauvage, S.,
596 Poulain, L., Sciare, J., Bonsang, B., 2012. Total OH reactivity measurements in Paris during the
597 2010 MEGAPOLI winter campaign. Atmospheric Chemistry and Physics 12, 9593-9612.
598 Dominutti, P., Keita, S., Bahino, J., Colomb, A., Liousse, C., Yoboué, V., Galy-Lacaux, C., Morris,
599 E., Bouvier, L., Sauvage, S., Borbon, A., 2019. Anthropogenic VOCs in Abidjan, southern West
600 Africa: from source quantification to atmospheric impacts. Atmos. Chem. Phys. 19, 11721-11741.
601 Ehhalt, D.H., Rohrer, F., 2000. Dependence of the OH concentration on solar UV. Journal of
602 Geophysical Research 105, 3565-3571.
603 Ehhalt, D.H., Rohrer, F., Wahner, A., 2015. Tropospheric Chemistry and Composition |Oxidizing
604 Capacity. Encyclopedia of Atmospheric Sciences 6, 243-250.
605 Elshorbany, Y.F., Kurtenbach, R., Wiesen, P., Lissi, E., Rubio, M., Villena, G., Gramsch, E.,
606 Rickard, A.R., Pilling, M.J., Kleffmann, J., 2009. Oxidation capacity of the city air of Santiago,
607 Chile. Atmospheric Chemistry and Physics 9, 2257-2273.
608 Ensberg, J.J., Hayes, P.L., Jimenez, J.L., Gilman, J.B., Kuster, W.C., de Gouw, J.A., Holloway,
609 J.S., Gordon, T.D., Jathar, S., Robinson, A.L., Seinfeld, J.H., 2014. Emission factor ratios, SOA
610 mass yields, and the impact of vehicular emissions on SOA formation. Atmospheric Chemistry

611 and Physics 14, 2383-2397.
612 Feng, T., Zhao, S., Bei, N., Wu, J., Liu, S., Li, X., Liu, L., Qian, Y., Yang, Q., Wang, Y., Zhou, W.,
613 Cao, J., Li, G., 2019. Secondary organic aerosol enhanced by increasing atmospheric oxidizing
614 capacity in Beijing–Tianjin–Hebei (BTH), China. Atmos. Chem. Phys. 19, 7429-7443.
615 Ferracci, V., Heimann, I., Abraham, N.L., Pyle, J.A., Archibald, A.T., 2018. Global modelling of
616 the total OH reactivity: investigations on the "missing" OH sink and its atmospheric implications.
617 Atmospheric Chemistry and Physics 18, 7109-7129.
618 Fuchs, H., Tan, Z., Lu, K., Bohn, B., Broch, S., Brown, S.S., Dong, H., Gomm, S., Häseler, R., He,
619 L., Hofzumahaus, A., Holland, F., Li, X., Liu, Y., Lu, S., Min, K.-E., Rohrer, F., Shao, M., Wang,
620 B., Wang, M., Wu, Y., Zeng, L., Zhang, Y., Wahner, A., Zhang, Y., 2017. OH reactivity at a rural
621 site (Wangdu) in the North China Plain: contributions from OH reactants and experimental OH
622 budget. Atmospheric Chemistry and Physics 17, 645-661.
623 Geyer, A., Alicke, B., Konrad, S., Schmitz, T., Stutz, J., Platt, U., 2001. Chemistry and oxidation
624 capacity of the nitrate radical in the continental boundary layer near Berlin. Journal of
625 Geophysical Research: Atmospheres 106, 8013-8025.
626 Gilman, J.B., Lerner, B.M., Kuster, W.C., Goldan, P.D., Warneke, C., Veres, P.R., Roberts, J.M., de
627 Gouw, J.A., Burling, I.R., Yokelson, R.J., 2015. Biomass burning emissions and potential air
628 quality impacts of volatile organic compounds and other trace gases from fuels common in the US.
629 Atmospheric Chemistry and Physics 15, 13915-13938.
630 Guo, H., So, K.L., Simpson, I.J., Barletta, B., Meinardi, S., Blake, D.R., 2007. C1–C8 volatile
631 organic compounds in the atmosphere of Hong Kong: Overview of atmospheric processing and
632 source apportionment. Atmospheric Environment 41, 1456-1472.
633 Han, D., Wang, Z., Cheng, J., Wang, Q., Chen, X., Wang, H., 2017. Volatile organic compounds
634 (VOCs) during non-haze and haze days in Shanghai: characterization and secondary organic
635 aerosol (SOA) formation. Environ Sci Pollut Res Int 24, 18619-18629.
636 Han, D.M., Gao, S., Fu, Q.Y., Cheng, J.P., Chen, X.J., Xu, H., Liang, S., Zhou, Y., Ma, Y.N., 2018.
637 Do volatile organic compounds (VOCs) emitted from petrochemical industries affect regional
638 PM2.5? Atmospheric Research 209, 123-130.
639 Hayes, P.L., Ortega, A.M., Cubison, M.J., Froyd, K.D., Zhao, Y., Cliff, S.S., Hu, W.W., Toohey,
640 D.W., Flynn, J.H., Lefer, B.L., Grossberg, N., Alvarez, S., Rappenglück, B., Taylor, J.W., Allan,

641 J.D., Holloway, J.S., Gilman, J.B., Kuster, W.C., de Gouw, J.A., Massoli, P., Zhang, X., Liu, J.,
642 Weber, R.J., Corrigan, A.L., Russell, L.M., Isaacman, G., Worton, D.R., Kreisberg, N.M.,
643 Goldstein, A.H., Thalman, R., Waxman, E.M., Volkamer, R., Lin, Y.H., Surratt, J.D., Kleindienst,
644 T.E., Offenberg, J.H., Dusanter, S., Griffith, S., Stevens, P.S., Brioude, J., Angevine, W.M.,
645 Jimenez, J.L., 2013. Organic aerosol composition and sources in Pasadena, California, during the
646 2010 CalNex campaign. Journal of Geophysical Research: Atmospheres 118, 9233-9257.
647 Jang, M., Czoschke, N.M., Northcross, A.L., Cao, G., Shaof, D., 2006. SOA Formation from
648 Partitioning and Heterogeneous Reactions: Model Study in the Presence of Inorganic Species.
649 Environmental Science & Technology 40, 3013-3022.
650 Jimenez, J.L., Canagaratna, M.R., Donahue, N.M., Prevot, A.S.H., Zhang, Q., Kroll, J.H., DeCarlo,
651 P.F., Allan, J.D., Coe, H., Ng, N.L., Aiken, A.C., Docherty, K.S., Ulbrich, I.M., Grieshop, A.P.,
652 Robinson, A.L., Duplissy, J., Smith, J.D., Wilson, K.R., Lanz, V.A., Hueglin, C., Sun, Y.L., Tian, J.,
653 Laaksonen, A., Raatikainen, T., Rautiainen, J., Vaattovaara, P., Ehn, M., Kulmala, M., Tomlinson,
654 J.M., Collins, D.R., Cubison, M.J., Dunlea, J., Huffman, J.A., Onasch, T.B., Alfarra, M.R.,
655 Williams, P.I., Bower, K., Kondo, Y., Schneider, J., Drewnick, F., Borrmann, S., Weimer, S.,
656 Demerjian, K., Salcedo, D., Cottrell, L., Griffin, R., Takami, A., Miyoshi, T., Hatakeyama, S.,
657 Shimono, A., Sun, J.Y., Zhang, Y.M., Dzepina, K., Kimmel, J.R., Sueper, D., Jayne, J.T., Herndon,
658 S.C., Trimborn, A.M., Williams, L.R., Wood, E.C., Middlebrook, A.M., Kolb, C.E., Baltensperger,
659 U., Worsnop, D.R., 2009. Evolution of Organic Aerosols in the Atmosphere. Science 326,
660 1525-1529.
661 Kirchner, F., Jeanneret, F., Clappier, A., Krüger, B., van den Bergh, H., Calpini, B., 2001. Total
662 VOC reactivity in the planetary boundary layer: 2. A new indicator for determining the sensitivity
663 of the ozone production to VOC and NOx. Journal of Geophysical Research: Atmospheres 106,
664 3095-3110.
665 Kleinman, L.I., Springston, S.R., Daum, P.H., Lee, Y.N., Nunnermacker, L.J., Senum, G.I., Wang,
666 J., Weinstein-Lloyd, J., Alexander, M.L., Hubbe, J., Ortega, J., Canagaratna, M.R., Jayne, J.T.,
667 2008. The time evolution of aerosol composition over the Mexico City plateau. Atmospheric
668 Chemistry and Physics 8, 1559-1575.
669 Kovacs, T.A., Brune, W.H., Harder, H., Martinez, M., Simpas, J.B., Frost, G.J., Williams, E.,
670 Jobson, T., Stroud, C., Young, V., Fried, A., Wert, B., 2003. Direct measurements of urban OH

671 reactivity during Nashville SOS in summer 1999. Journal of Environmental Monitoring 5, 68-74.
672 Kroll, J.H., Seinfeld, J.H., 2008. Chemistry of secondary organic aerosol: Formation and evolution
673 of low-volatility organics in the atmosphere. Atmospheric Environment 42, 3593-3624.
674 Lambe, A.T., Onasch, T.B., Croasdale, D.R., Wright, J.P., Martin, A.T., Franklin, J.P., Massoli, P.,
675 Kroll, J.H., Canagaratna, M.R., Brune, W.H., Worsnop, D.R., Davidovits, P., 2012. Transitions
676 from Functionalization to Fragmentation Reactions of Laboratory Secondary Organic Aerosol
677 (SOA) Generated from the OH Oxidation of Alkane Precursors. Environmental Science &
678 Technology 46, 5430-5437.
679 Laurila, T., Hakola, H., 1996. Seasonal cycle of C2-C5 hydrocarbons over the Baltic Sea and
680 Northern Finland. Atmospheric Environment 30, 1597-1607.
681 Levy, H., 1971. Normal Atmosphere - Large Radical and Formaldehyde Concentrations Predicted.
682 Science 173, 141-143.
683 Li, B., Ho, S.S.H., Gong, S., Ni, J., Li, H., Han, L., Yang, Y., Qi, Y., Zhao, D., 2019a.
684 Characterization of VOCs and their related atmospheric processes in a central Chinese city during
685 severe ozone pollution periods. Atmospheric Chemistry and Physics 19, 617-638.
686 Li, K., Jacob, D.J., Liao, H., Shen, L., Zhang, Q., Bates, K.H., 2019b. Anthropogenic drivers of
687 2013-2017 trends in summer surface ozone in China. Proc Natl Acad Sci US A 116, 422-427.
688 Li, M., Zhang, Q., Zheng, B., Tong, D., Lei, Y., Liu, F., Hong, C., Kang, S., Yan, L., Zhang, Y., Bo,
689 Y., Su, H., Cheng, Y., He, K., 2019c. Persistent growth of anthropogenic non-methane volatile
690 organic compound (NMVOC) emissions in China during 1990–2017: drivers, speciation and
691 ozone formation potential. Atmospheric Chemistry and Physics 19, 8897-8913.
692 Li, Z., Xue, L., Yang, X., Zha, Q., Tham, Y.J., Yan, C., Louie, P.K.K., Luk, C.W.Y., Wang, T.,
693 Wang, W., 2018. Oxidizing capacity of the rural atmosphere in Hong Kong, Southern China.
694 Science of the Total Environment 612, 1114-1122.
695 Liebmann, J.M., Muller, J.B.A., Kubistin, D., Claude, A., Holla, R., Plass-Dülmer, C., Lelieveld,
696 J., Crowley, J.N., 2018. Direct measurements of NO_3 reactivity in and above the boundary layer of
697 a mountaintop site: identification of reactive trace gases and comparison with OH reactivity.
698 Atmospheric Chemistry and Physics 18, 12045-12059.
699 Liu, C.T., Ma, Z.B., Mu, Y.J., Liu, J.F., Zhang, C.L., Zhang, Y.Y., Liu, P.F., Zhang, H.X., 2017.
700 The levels, variation characteristics, and sources of atmospheric non-methane hydrocarbon

compounds during wintertime in Beijing, China. Atmospheric Chemistry and Physics 17, 10633-10649.

Liu, Y., Shao, M., Lu, S.H., Liao, C.C., Wang, J.L., Chen, G., 2008. Volatile organic compound (VOC) measurements in the pearl river delta (PRD) region, China. Atmospheric Chemistry and Physics 8, 1531-1545.

Liu, Z., Hu, B., Wang, L., Wu, F., Gao, W., Wang, Y., 2015. Seasonal and diurnal variation in particulate matter (PM_{10} and $PM_{2.5}$) at an urban site of Beijing: analyses from a 9-year study. Environmental Science & Pollution Research 22, 627-642.

Lou, S., Holland, F., Rohrer, F., Lu, K., Bohn, B., Brauers, T., Chang, C.C., Fuchs, H., Häseler, R., Kita, K., Kondo, Y., Li, X., Shao, M., Zeng, L., Wahner, A., Zhang, Y., Wang, W., Hofzumahaus, A., 2010. Atmospheric OH reactivities in the Pearl River Delta-China in summer 2006: measurement and model results. Atmospheric Chemistry and Physics 10, 11243-11260.

Lu, K.D., Hofzumahaus, A., Holland, F., Bohn, B., Brauers, T., Fuchs, H., Hu, M., Häseler, R., Kita, K., Kondo, Y., Li, X., Lou, S.R., Oebel, A., Shao, M., Zeng, L.M., Wahner, A., Zhu, T., Zhang, Y.H., Rohrer, F., 2013. Missing OH source in a suburban environment near Beijing: observed and modelled OH and HO_2 concentrations in summer 2006. Atmospheric Chemistry and Physics 13, 1057-1080.

Lyu, X., Wang, N., Guo, H., Xue, L., Jiang, F., Zeren, Y., Cheng, H., Cai, Z., Han, L., Zhou, Y., 2019. Causes of a continuous summertime O_3 pollution event in Jinan, a central city in the North China Plain. Atmospheric Chemistry and Physics 19, 3025-3042.

Mao, J., Ren, X., Chen, S., Brune, W.H., Chen, Z., Martinez, M., Harder, H., Lefer, B., Rappenglück, B., Flynn, J., Leuchner, M., 2010. Atmospheric oxidation capacity in the summer of Houston 2006: Comparison with summer measurements in other metropolitan studies. Atmospheric Environment 44, 4107-4115.

McKeen, S.A., Liu, S.C., Hsie, E.Y., Lin, X., Bradshaw, J.D., Smyth, S., Gregory, G.L., Blake, D.R., 1996. Hydrocarbon ratios during PEM-WEST A: A model perspective. Journal of Geophysical Research: Atmospheres 101, 2087-2109.

Murray, K.K., Boyd, R.K., Eberlin, M.N., Langley, G.J., Li, L., Naito, Y., 2013. Definitions of terms relating to mass spectrometry (IUPAC Recommendations 2013). Pure and Applied Chemistry 85, 1515-1609.

731 Nelson, P.F., Quigley, S.M., 1983. The m,p-xylenes:ethylbenzene ratio. A technique for estimating
732 hydrocarbon age in ambient atmospheres. Atmospheric Environment 17, 659-662.
733 Parrish, D.D., Stohl, A., Forster, C., Atlas, E.L., Blake, D.R., Goldan, P.D., Kuster, W.C., de Gouw,
734 J.A., 2007. Effects of mixing on evolution of hydrocarbon ratios in the troposphere. Journal of
735 Geophysical Research: Atmospheres 112.
736 Parrish, D.D., Trainer, M., Young, V., Goldan, P.D., Kuster, W.C., Jobson, B.T., Fehsenfeld, F.C.,
737 Lonneman, W.A., Zika, R.D., Farmer, C.T., Riemer, D.D., Rodgers, M.O., 1998. Internal
738 consistency tests for evaluation of measurements of anthropogenic hydrocarbons in the
739 troposphere. Journal of Geophysical Research: Atmospheres 103, 22339-22359.
740 Pfannerstill, E.Y., Wang, N.J., Edtbauer, A., Bourtsoukidis, E., Crowley, J.N., Dienhart, D., Eger,
741 P.G., Ernle, L., Fischer, H., Hottmann, B., Paris, J.D., Stonner, C., Tadic, I., Walter, D., Williams,
742 J., 2019. Shipborne measurements of total OH reactivity around the Arabian Peninsula and its role
743 in ozone chemistry. Atmospheric Chemistry and Physics 19, 11501-11523.
744 Prinn, R.G., 2003. The Cleansing Capacity of the Atmosphere. Annual Review of Environment
745 and Resources 28, 29-57.
746 Ren, X., 2003. HOx concentrations and OH reactivity observations in New York City during
747 PMTACS-NY2001. Atmospheric Environment 37, 3627-3637.
748 Ren, X., Brune, W.H., Mao, J., Mitchell, M.J., Lesher, R.L., Simpas, J.B., Metcalf, A.R., Schwab,
749 J.J., Cai, C., Li, Y., 2006. Behavior of OH and HO_2 in the winter atmosphere in New York City.
750 Atmospheric Environment 40, 252-263.
751 Roberts, J.M., Fehsenfeld, F.C., Liu, S.C., Bollinger, M., HAHN, C., Albritton, D.L., Sievers, R.E.,
752 1984. Measurements of aromatic hydrocarbon ratios and NOx concentrations in the rural
753 troposphere Observation of air mass photochemical aging and NOx removal. Atmospheric
754 Environment 18, 2421-2432.
755 Seinfeld, J.H., 1989. Urban Air Pollution: State of the Science. Science 243, 745-752.
756 Sheehy, P.M., Volkamer, R., Molina, L.T., Molina, M.J., 2010. Oxidative capacity of the Mexico
757 City atmosphere – Part 2: A ROx radical cycling perspective. Atmospheric Chemistry and Physics
758 10, 6993-7008.
759 Sinha, V., Williams, J., Diesch, J.M., Drewnick, F., Martinez, M., Harder, H., Regelin, E., Kubistin,
760 D., Bozem, H., Hosaynali-Beygi, Z., Fischer, H., Andrés-Hernández, M.D., Kartal, D., Adame,

761 J.A., Lelieveld, J., 2012. Constraints on instantaneous ozone production rates and regimes during
762 DOMINO derived using in-situ OH reactivity measurements. Atmospheric Chemistry and Physics
763 12, 7269-7283.
764 So, K.L., Wang, T., 2004. C3-C12 non-methane hydrocarbons in subtropical Hong Kong:
765 spatial-temporal variations, source-receptor relationships and photochemical reactivity. Science of
766 the Total Environment 328, 161-174.
767 Sommariva, R., de Gouw, J.A., Trainer, M., Atlas, E., Goldan, P.D., Kuster, W.C., Warneke, C.,
768 Fehsenfeld, F.C., 2011. Emissions and photochemistry of oxygenated VOCs in urban plumes in
769 the Northeastern United States. Atmospheric Chemistry and Physics 11, 7081-7096.
770 Song, M.D., Tan, Q.W., Feng, M., Qu, Y., Liu, X.G., An, J.L., Zhang, Y.H., 2018. Source
771 Apportionment and Secondary Transformation of Atmospheric Nonmethane Hydrocarbons in
772 Chengdu, Southwest China. Journal of Geophysical Research-Atmospheres 123, 9741-9763.
773 Sun, J., Wu, F., Hu, B., Tang, G., Zhang, J., Wang, Y., 2016a. VOC characteristics, emissions and
774 contributions to SOA formation during hazy episodes. Atmospheric Environment 141, 560-570.
775 Sun, W., Shao, M., Granier, C., Liu, Y., Ye, C.S., Zheng, J.Y., 2018. Long-Term Trends of
776 Anthropogenic SO_2, NOx, CO, and NMVOCs Emissions in China. Earth's Future 6, 1112-1133.
777 Sun, Y., Jiang, Q., Xu, Y., Ma, Y., Zhang, Y., Liu, X., Li, W., Wang, F., Li, J., Wang, P., Li, Z.,
778 2016b. Aerosol characterization over the North China Plain: Haze life cycle and biomass burning
779 impacts in summer. Journal of Geophysical Research: Atmospheres 121, 2508-2521.
780 Tan, Z., Lu, K., Jiang, M., Su, R., Wang, H., Lou, S., Fu, Q., Zhai, C., Tan, Q., Yue, D., Chen, D.,
781 Wang, Z., Xie, S., Zeng, L., Zhang, Y., 2019. Daytime atmospheric oxidation capacity in four
782 Chinese megacities during the photochemically polluted season: a case study based on box model
783 simulation. Atmospheric Chemistry and Physics 19, 3493-3513.
784 Tang, G., Wang, Y., Li, X., Ji, D., Hsu, S., Gao, X., 2012. Spatial-temporal variations in surface
785 ozone in Northern China as observed during 2009–2010 and possible implications for future air
786 quality control strategies. Atmospheric Chemistry and Physics 12, 2757-2776.
787 Tham, Y.J., Wang, Z., Li, Q., Wang, W., Wang, X., Lu, K., Ma, N., Yan, C., Kecorius, S.,
788 Wiedensohler, A., Zhang, Y., Wang, T., 2018. Heterogeneous N_2O_5 uptake coefficient and
789 production yield of $ClNO_2$ in polluted northern China: roles of aerosol water content and chemical
790 composition. Atmospheric Chemistry and Physics 18, 13155-13171.

Volkamer, R., Jimenez, J.L., San Martini, F., Dzepina, K., Zhang, Q., Salcedo, D., Molina, L.T., Worsnop, D.R., Molina, M.J., 2006. Secondary organic aerosol formation from anthropogenic air pollution: Rapid and higher than expected. Geophysical Research Letters 33.

Wang, M., Shao, M., Chen, W., Lu, S., Liu, Y., Yuan, B., Zhang, Q., Zhang, Q., Chang, C.C., Wang, B., Zeng, L., Hu, M., Yang, Y., Li, Y., 2015a. Trends of non-methane hydrocarbons (NMHC) emissions in Beijing during 2002–2013. Atmospheric Chemistry and Physics 15, 1489-1502.

Wang, T., Hendrick, F., Wang, P., Tang, G., Clémer, K., Yu, H., Fayt, C., Hermans, C., Gielen, C., Müller, J.F., Pinardi, G., Theys, N., Brenot, H., Van Roozendael, M., 2014a. Evaluation of tropospheric SO_2 retrieved from MAX-DOAS measurements in Xianghe, China. Atmospheric Chemistry and Physics 14, 11149-11164.

Wang, W., Li, X., Shao, M., Hu, M., Zeng, L., Wu, Y., Tan, T., 2019a. The impact of aerosols on photolysis frequencies and ozone production in Beijing during the 4-year period 2012–2015. Atmospheric Chemistry and Physics 19, 9413-9429.

Wang, Y., Hu, B., Tang, G., Ji, D., Zhang, H., Bai, J., Wang, X., Wang, Y., 2013. Characteristics of ozone and its precursors in Northern China: A comparative study of three sites. Atmospheric Research 132-133, 450-459.

Wang, Y., Wang, Y., Wang, L., Petäjä, T., Zha, Q., Gong, C., Li, S., Pan, Y., Hu, B., Xin, J., Kulmala, M., 2019b. Increased inorganic aerosol fraction contributes to air pollution and haze in China. Atmos. Chem. Phys. 19, 5881-5888.

Wang, Y.H., Hu, B., Ji, D.S., Liu, Z.R., Tang, G.Q., Xin, J.Y., Zhang, H.X., Song, T., Wang, L.L., Gao, W.K., Wang, X.K., Wang, Y.S., 2014b. Ozone weekend effects in the Beijing–Tianjin–Hebei metropolitan area, China. Atmospheric Chemistry and Physics 14, 2419-2429.

Wang, Y.H., Liu, Z.R., Zhang, J.K., Hu, B., Ji, D.S., Yu, Y.C., Wang, Y.S., 2015b. Aerosol physicochemical properties and implications for visibility during an intense haze episode during winter in Beijing. Atmos. Chem. Phys. 15, 3205-3215.

Warneke, C., McKeen, S.A., de Gouw, J.A., Goldan, P.D., Kuster, W.C., Holloway, J.S., Williams, E.J., Lerner, B.M., Parrish, D.D., Trainer, M., Fehsenfeld, F.C., Kato, S., Atlas, E.L., Baker, A., Blake, D.R., 2007. Determination of urban volatile organic compound emission ratios and comparison with an emissions database. Journal of Geophysical Research: Atmospheres 112, D10S47.

Whalley, L.K., Stone, D., Bandy, B., Dunmore, R., Hamilton, J.F., Hopkins, J., Lee, J.D., Lewis, A.C., Heard, D.E., 2016. Atmospheric OH reactivity in central London: observations, model predictions and estimates of in situ ozone production. Atmospheric Chemistry and Physics 16, 2109-2122.

Williams, J., Keßel, S.U., Nölscher, A.C., Yang, Y., Lee, Y., Yáñez-Serrano, A.M., Wolff, S., Kesselmeier, J., Klüpfel, T., Lelieveld, J., Shao, M., 2016. Opposite OH reactivity and ozone cycles in the Amazon rainforest and megacity Beijing: Subversion of biospheric oxidant control by anthropogenic emissions. Atmospheric Environment 125, 112-118.

Wu, R., Xie, S., 2017. Spatial Distribution of Ozone Formation in China Derived from Emissions of Speciated Volatile Organic Compounds. Environmental Science & Technology 51, 2574-2583.

Wu, R., Xie, S., 2018. Spatial Distribution of Secondary Organic Aerosol Formation Potential in China Derived from Speciated Anthropogenic Volatile Organic Compound Emissions. Environmental Science & Technology 52, 8146-8156.

Xin, J., Wang, Y., Wang, L., Tang, G., Sun, Y., Pan, Y., Ji, D., 2012. Reductions of PM2.5 in Beijing-Tianjin-Hebei urban agglomerations during the 2008 Olympic Games. Advances in Atmospheric Sciences 29, 1330-1342.

Xin, J.Y., Wang, Y.S., Pan, Y.P., Ji, D.S., Liu, Z.R., Wen, T.X., Wang, Y.H., Li, X.R., Sun, Y., Sun, J., Wang, P.C., Wang, G.H., Wang, X.M., Cong, Z.Y., Song, T., Hu, B., Wang, L.L., Tang, G.Q., Gao, W.K., Guo, Y.H., Miao, H.Y., Tian, S.L., Wang, L., 2015. The Campaign on Atmospheric Aerosol Research Network of China Care-China. Bulletin of the American Meteorological Society 96, 1137-1155.

Xu, J., Ma, J.Z., Zhang, X.L., Xu, X.B., Xu, X.F., Lin, W.L., Wang, Y., Meng, W., Ma, Z.Q., 2011. Measurements of ozone and its precursors in Beijing during summertime: impact of urban plumes on ozone pollution in downwind rural areas. Atmospheric Chemistry and Physics 11, 12241-12252.

Xue, L., Gu, R., Wang, T., Wang, X., Saunders, S., Blake, D., Louie, P.K.K., Luk, C.W.Y., Simpson, I., Xu, Z., Wang, Z., Gao, Y., Lee, S., Mellouki, A., Wang, W., 2016. Oxidative capacity and radical chemistry in the polluted atmosphere of Hong Kong and Pearl River Delta region: analysis of a severe photochemical smog episode. Atmospheric Chemistry and Physics 16, 9891-9903.

Xue, Y., Ho, S.S.H., Huang, Y., Li, B., Wang, L., Dai, W., Cao, J., Lee, S., 2017. Source apportionment of VOCs and their impacts on surface ozone in an industry city of Baoji, Northwestern China. Sci Rep 7, 9979.

Yang, Y., Ji, D., Sun, J., Wang, Y., Yao, D., Zhao, S., Yu, X., Zeng, L., Zhang, R., Zhang, H., Wang, Y., Wang, Y., 2019a. Ambient volatile organic compounds in a suburban site between Beijing and Tianjin: Concentration levels, source apportionment and health risk assessment. Science of the Total Environment 695, 133889.

Yang, Y., Shao, M., Keßel, S., Li, Y., Lu, K., Lu, S., Williams, J., Zhang, Y., Zeng, L., Nölscher, A.C., Wu, Y., Wang, X., Zheng, J., 2017. How the OH reactivity affects the ozone production efficiency: case studies in Beijing and Heshan, China. Atmospheric Chemistry and Physics 17, 7127-7142.

Yang, Y., Shao, M., Wang, X., Nölscher, A.C., Kessel, S., Guenther, A., Williams, J., 2016. Towards a quantitative understanding of total OH reactivity: A review. Atmospheric Environment 134, 147-161.

Yang, Y., Zhou, M., Langerock, B., Sha, M.K., Hermans, C., Wang, T., Ji, D., Vigouroux, C., Kumps, N., Wang, G., De Mazière, M., Wang, P., 2019b. A new site: ground-based FTIR XCO_2, XCH_4 and XCO measurements at Xianghe, China. Earth Syst. Sci. Data Discuss. 2019, 1-27.

Yuan, B., Hu, W.W., Shao, M., Wang, M., Chen, W.T., Lu, S.H., Zeng, L.M., Hu, M., 2013. VOC emissions, evolutions and contributions to SOA formation at a receptor site in eastern China. Atmospheric Chemistry and Physics 13, 8815-8832.

Yuan, B., Shao, M., de Gouw, J., Parrish, D.D., Lu, S., Wang, M., Zeng, L., Zhang, Q., Song, Y., Zhang, J., Hu, M., 2012. Volatile organic compounds (VOCs) in urban air: How chemistry affects the interpretation of positive matrix factorization (PMF) analysis. Journal of Geophysical Research: Atmospheres 117, 24302.

Zhang, J., Wang, T., Chameides, W.L., Cardelino, C., Blake, D.R., Streets, D.G., 2008. Source characteristics of volatile organic compounds during high ozone episodes in Hong Kong, Southern China. Atmospheric Chemistry and Physics 8, 4983-4996.

Zhang, Z., Wang, H., Chen, D., Li, Q., Thai, P., Gong, D., Li, Y., Zhang, C., Gu, Y., Zhou, L., Morawska, L., Wang, B., 2017. Emission characteristics of volatile organic compounds and their secondary organic aerosol formation potentials from a petroleum refinery in Pearl River Delta,

881 China. Science of the Total Environment 584-585, 1162-1174.
882 Zheng, B., Tong, D., Li, M., Liu, F., Hong, C., Geng, G., Li, H., Li, X., Peng, L., Qi, J., Yan, L.,
883 Zhang, Y., Zhao, H., Zheng, Y., He, K., Zhang, Q., 2018. Trends in China's anthropogenic
884 emissions since 2010 as the consequence of clean air actions. Atmospheric Chemistry and Physics
885 18, 14095-14111.
886 Zheng, J., Hu, M., Zhang, R., Yue, D., Wang, Z., Guo, S., Li, X., Bohn, B., Shao, M., He, L., 2011.
887 Measurements of gaseous H_2SO_4 by AP-ID-CIMS during CAREBeijing 2008 Campaign.
888 Atmospheric Chemistry and Physics 11, 7755-7765.
889 Zhu, J., Wang, S., Wang, H., Jing, S., Lou, S., Saiz-Lopez, A., Zhou, B., 2020. Observationally
890 constrained modeling of atmospheric oxidation capacity and photochemical reactivity in Shanghai,
891 China. Atmos. Chem. Phys. 20, 1217-1232.
892 Zou, Y., Deng, X.J., Zhu, D., Gong, D.C., Wang, H., Li, F., Tan, H.B., Deng, T., Mai, B.R., Liu,
893 X.T., Wang, B.G., 2015. Characteristics of 1 year of observational data of VOCs, NOx and O_3 at a
894 suburban site in Guangzhou, China. Atmospheric Chemistry and Physics 15, 6625-6636.
895

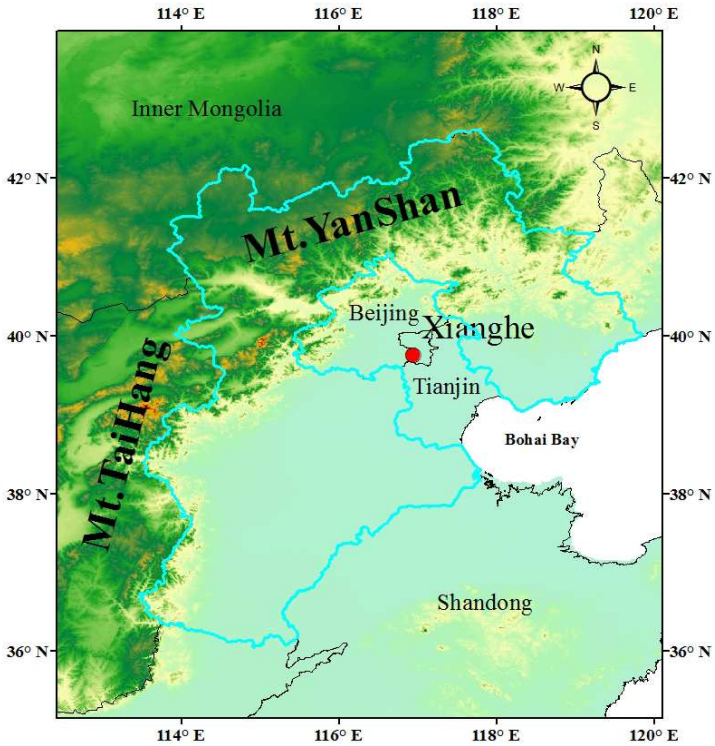

Figure 1. The location of the sampling site, marked with a red dot. The provincial boundary layer with a scale of 1:4,000,000 was obtained from the National Geomatics Center of China (http://www.ngcc.cn/ngcc/). Maps were generated based upon a geospatial analysis using ESRI ArcGIS software (version 10.1, http://www.esri.com/software/arcgis/arcgis-for-desktop).

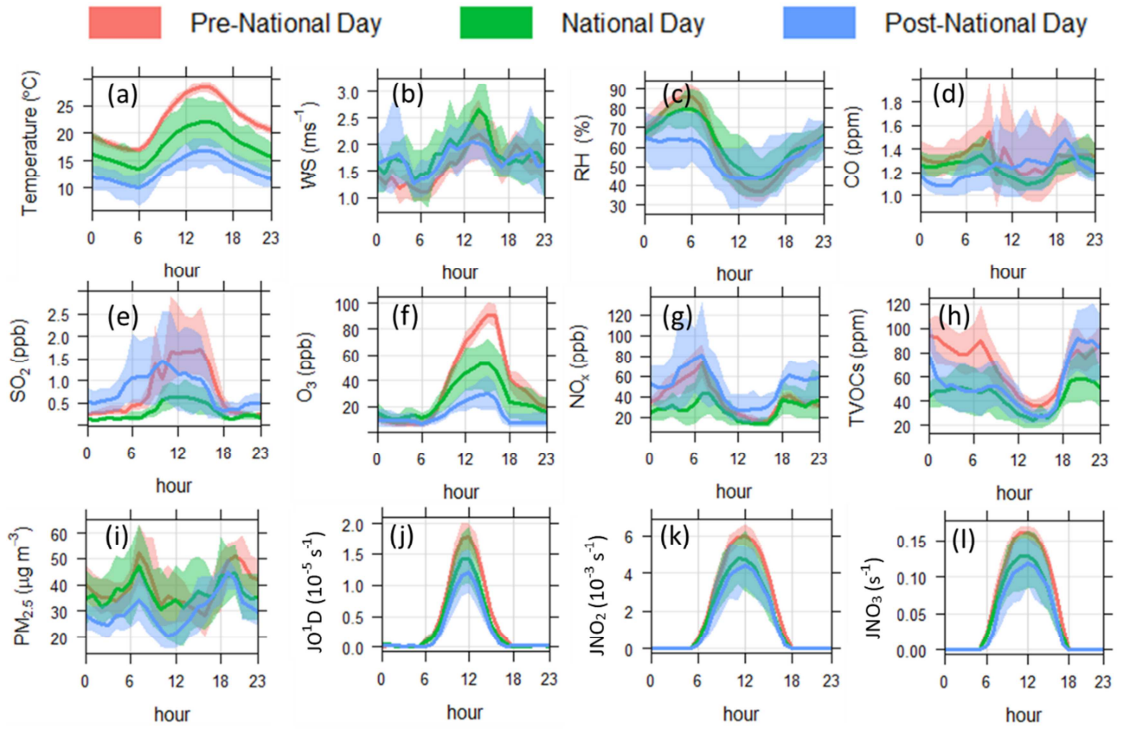

Figure 2. Diurnal variations (mean and 95% confidence interval of the mean) in the measured temperature (a), WS (b), RH (c), CO (d), SO_2 (e), O_3 (f), NO_x (g), TVOCs (h), $PM_{2.5}$ (i), JO^1D (j), JNO_2 (k) and JNO_3 (l) in Xianghe before, during, and after National Day 2019.

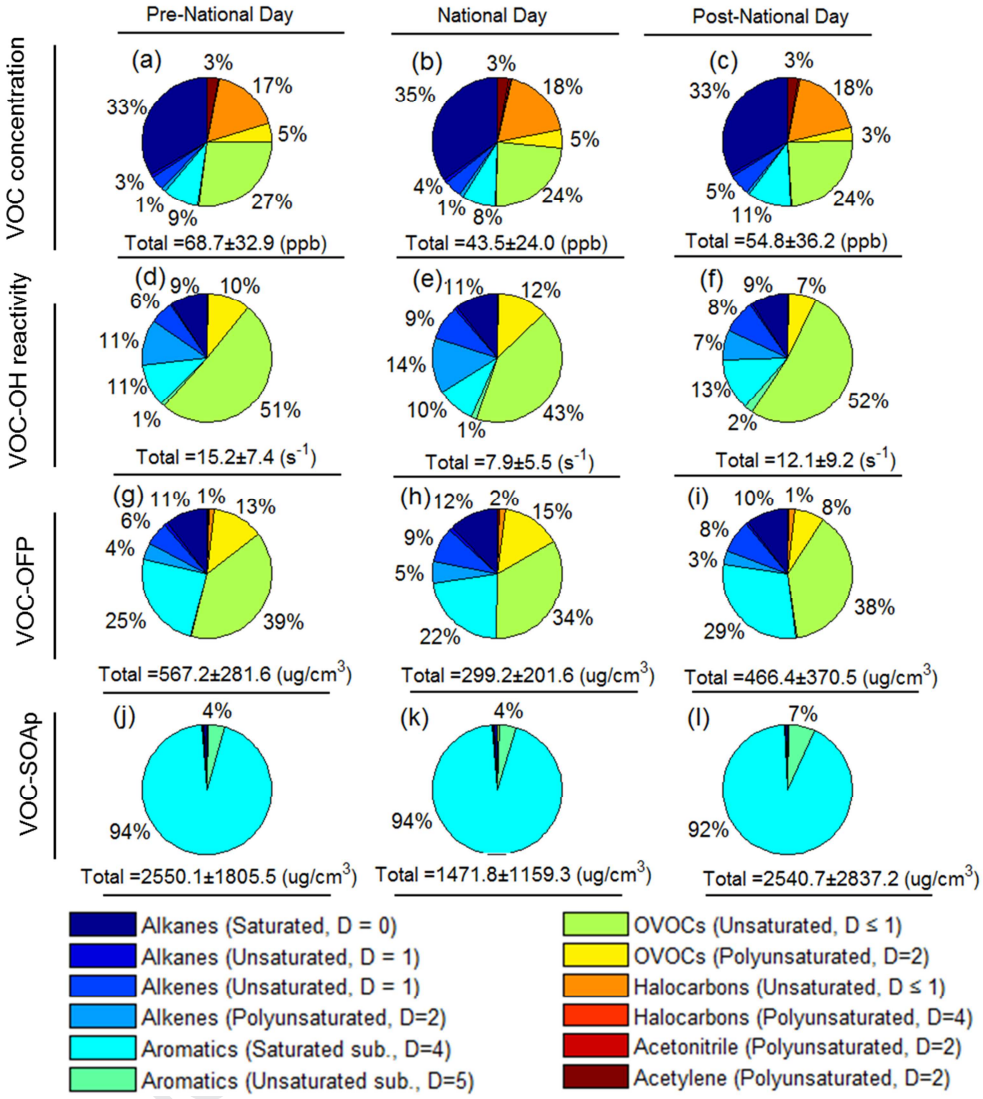

Figure 3. Contributions of VOCs to (a)-(c) the measured TVOC concentrations, (d)-(f) OH reactivity, (g)-(i) relative OFP and (j)-(l) relative SOAP in Xianghe before, during, and after National Day 2019. Absolute totals for each period are shown below each pie chart in the respective units. D= degree of unsaturation.

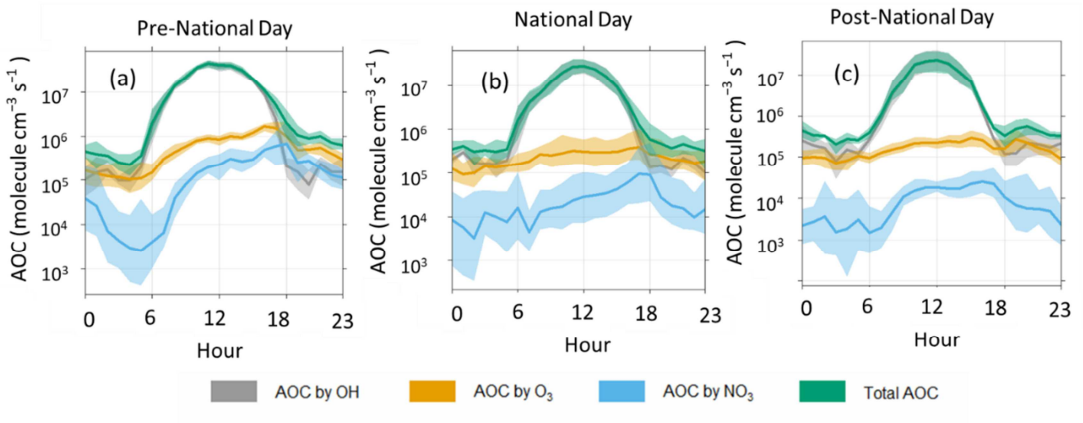

Figure 4. Mean diurnal variations in the calculated daytime AOC in Xianghe before, during, and after National Day 2019.

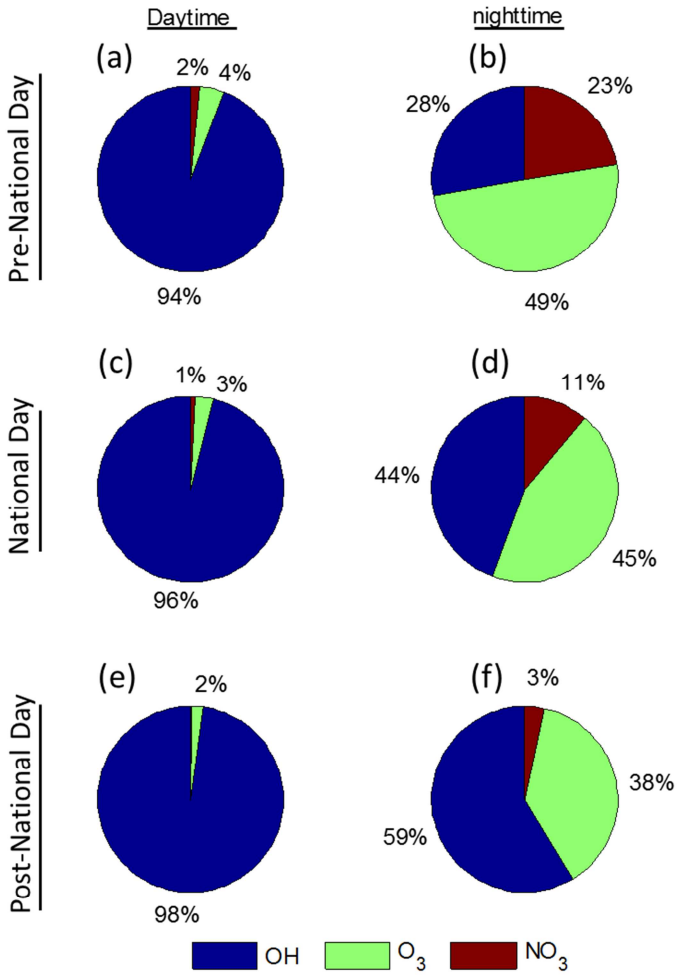

Figure 5. Comparison of the relative contributions of OH, O_3 and NO_3 to the daytime and nighttime integral of the AOC in Xianghe before, during, and after National Day 2019.

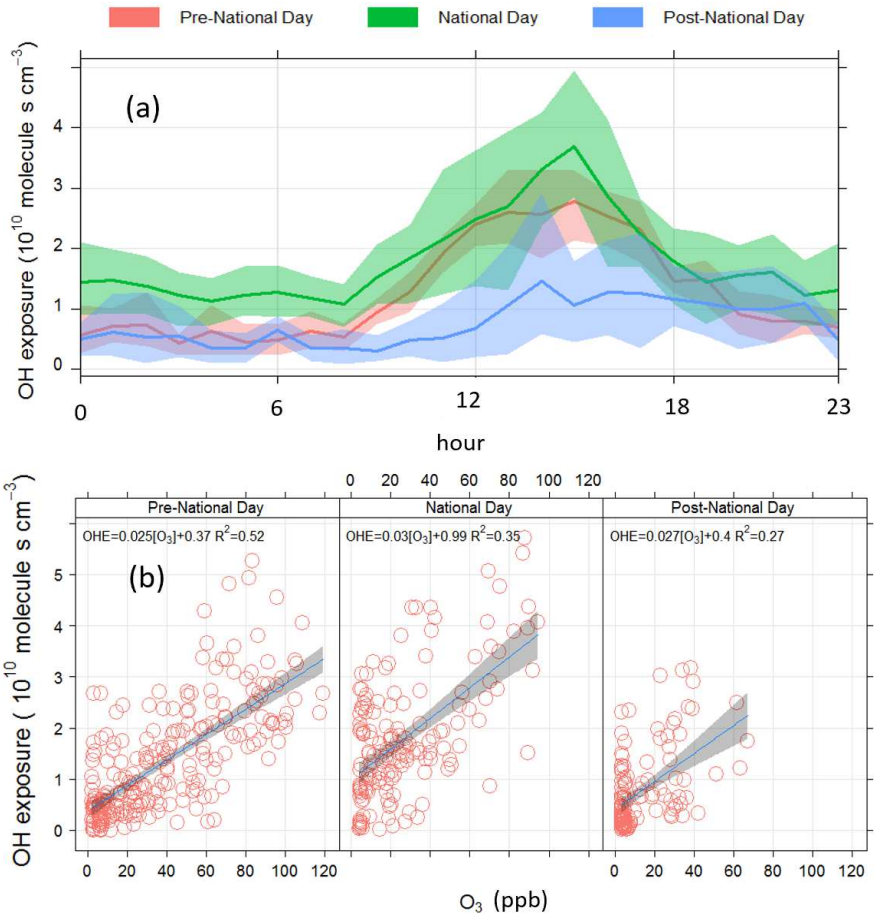

Figure 6. Daily variations in OH exposure (a) and scatter plots of OH exposure to O_3 (b) in Xianghe before, during, and after National Day 2019. OHE= OH exposure.

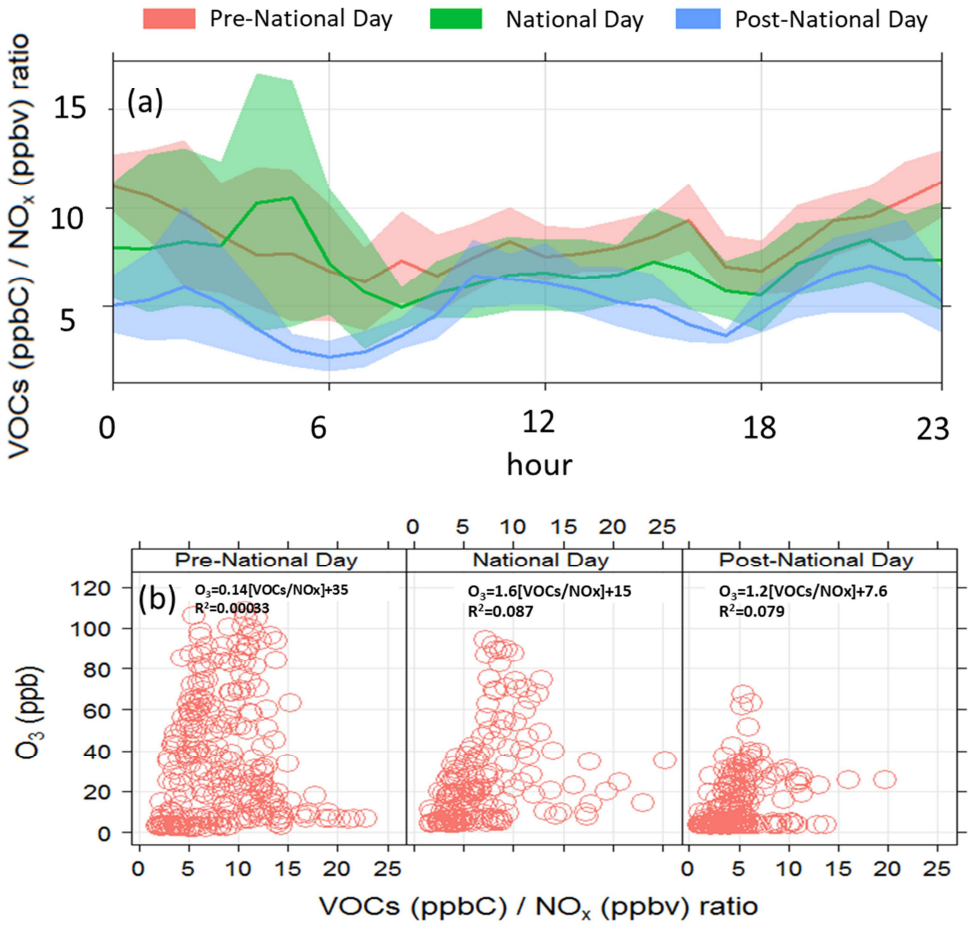

Figure 7. Daily variations in the VOC/NO_x ratio (a) and scatter plots of O_3 versus the VOC/NO_x ratio (b) in Xianghe before, during, and after National Day 2019.

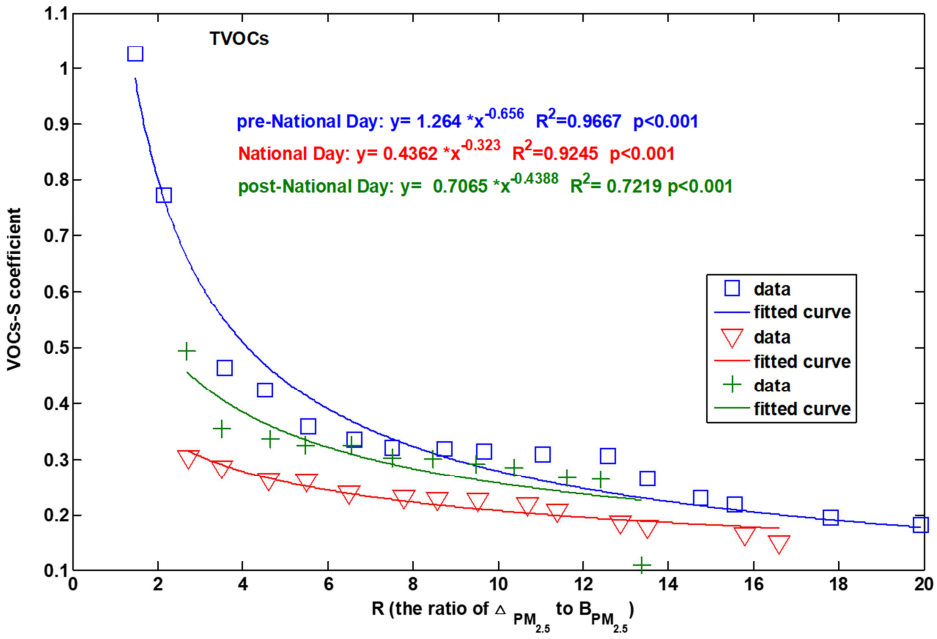

Figure 8. Trends of the VOC-S coefficient against R (the ratio of $\Delta_{PM_{2.5}}/B_{PM_{2.5}}$) for TVOCs in Xianghe before, during, and after National Day 2019.

Highlights:

- The significant decreases of atmospheric oxidation capacity and photochemical reactivity occurred during the National Day holiday
- Hydroxyl radical and O_3 correspondingly dominated the daytime and nighttime AOC during the sampling campaign
- Unsaturated species, the degree of unsaturation ≥1, are the major contributors to OH reactivity, O_3 and SOA formation
- VOCs were more sensitive to $PM_{2.5}$ in low-pollution domains and during the National Day holiday

Y.S.W designed the research. Y.Y and D.Y, S.M.Z, S.H.Y, D.S.J, Y.H.W conducted the measurements. Y.Y and Y.H.W interpreted the data and write the paper. All the authors commented on the paper.

Declaration of interests

☒ The authors declare that they have no known competing financial interests or personal relationships that could have appeared to influence the work reported in this paper.

☐The authors declare the following financial interests/personal relationships which may be considered as potential competing interests:

The authors declare that they have no conflict of interest